AN ABSTRACT OF THE THESIS OF

Kasidid Asumpinpong for the degree of Master of Science in Chemical Engineering presented on February 10, 2009

Title: Development of a Microchannel Device for Adsorption Cooling Application

Abstract approved:

_____

Gregory L. Rorrer

Single-layer and three-layer microchannel adsorption devices were fabricated by procedure that was newly developed. Aluminum was chosen for metal housing while the adsorption pair was silica gel and water. Each adsorption layer contained two layers of 250 µm-thick silica gel. Both silica gel layers opened to the same layer of adsorption channels. The layers of air flow channels were placed between two adsorption layers, including over the top and below the bottom adsorption layers. Each layer of adsorption channels and air flow channels contained array of six microchannels. Each microchannel was 400 µm tall, 5.8 mm wide and 4.4 cm long. The device was bonded by B-staged epoxy thin film at moderate temperature of 120°C. The overall dimensions of the fabricated device were 5 cm x 5 cm x 10.2 mm for the three-layer device. A maximum coefficient of performance (COP) of 0.506 was achieved at the evaporator temperature of 22°C, adsorption temperature of 23°C and desorption temperature of 50°C. The highest specific cooling power (SCP) obtained was 601 W/kg silica gel when desorption temperature was increased to 70°C The overall performance of the device improved slightly when the air flow rate was increased. The COP increased by a factor of 2.4 when the number of adsorption layers increased from 1 to 3. The results from simulation model agreed with the experimental results and also showed that both COP and SCP decreased drastically when evaporator temperature was far below the adsorption temperature.

Development of a Microchannel Device for Adsorption Cooling Application

by
Kasidid Asumpinpong

A THESIS

submitted to

Oregon State University

in partial fulfillment of
the requirements for the
degree of

Master of Science

Presented February 10, 2009
Commencement June 2009

Master of Science thesis of Kasidid Asumpinpong presented on February 10, 2009.

APPROVED:

Major Professor, representing Chemical Engineering

Head of the School of Chemical, Biological and Environmental Engineering

---

Dean of the Graduate School

I understand that my thesis will become part of the permanent collection of Oregon State University libraries. My signature below authorizes release of my thesis to any reader upon request.

Kasidid Asumpinpong, Author

ACKNOWLEDGEMENTS

This study was supported by the U.S. Army under the Tactical Energy Systems Program administered by the Oregon Nanoscience and Microtechnologies Institute. The author expresses sincere appreciation to the author's MS. Thesis advisor, Dr. Gregory Rorrer, for the invaluable discussions and guidance, continued support, and encouragement. As this study was collaboration between Oregon State University (OSU), and Pacific Northwest National Laboratory (PNNL), the author acknowledges Dr.Daniel Palo and Benjamin Roberts, who kindly allowed the author to use PNNL facilities and equipment, and assisted with the initial development of the microchannel architecture. The comments and help of colleagues in the Rorrer lab are gratefully acknowledged along with the recommendations from Thai students at OSU. Last but not least, a special thank goes to the author's parents and family who have been supportive through this degree, and for their long-distance advice.

TABLE OF CONTENTS

TABLE OF CONTENTS (Continued)

LIST OF FIGURES

LIST OF FIGURES (Continued)

LIST OF FIGURES (Continued)

LIST OF TABLES

LIST OF APPENDICES

LIST OF APPENDIX TABLES

Development of a Microchannel Device for Adsorption Cooling Application

Chapter 1 – Introduction and Literature Review

1.1 Background

The use of adsorption for heating/cooling has been known for long time. It was first reported by Plank and Kuprianoff[1] back in 1960.

An adsorption cooling system is known to be a cooling process which is not only capable for cooling down below room temperature but also environmentally friendly. There are no CFC refrigerants or hazardous chemicals used inside the cooling system. The working fluid, or adsorbate, is repeatedly adsorbed into and desorbed out of an adsorbent material in order to perform cooling. The adsorbent and adsorbate pairs that are typically used in adsorption cooling system as well as their operating temperatures are shown in Table 1.

Table 1. Adsorbent / adsorbate pairs and typical operating temperatures for adsorption cooling from the literature.

Adsorbent	Adsorbate	Cooling temperature	Desorption temperature	Reference
Silica gel	Water	7-20 ºC	> 50 ºC	[2], [3]
Zeolite	Water	7-20 ºC	> 100 ºC	[3]
Activated carbon	Methanol	< 0 ºC	80-120 ºC	[4]
Activated carbon	Ammonia	< 0 ºC	>80 ºC	[3], [4]

Energy supplied to the adsorption cooling system is more flexible than a conventional refrigeration system. The adsorption cooling system requires heat for the desorption stage. This heat supplied to the adsorption cooling system can be solar energy, waste heat or heat converted from electrical power. The compression refrigeration system generally requires only electrical power. Another advantage of adsorption cooling systems is that they have no moving parts.

The adsorption cooling process schematic is shown in Figure 1. There are four major mechanisms that occur during the cooling cycle: evaporation, adsorption,

desorption and condensation. Evaporation and adsorption simultaneously occur during adsorption stage, while desorption and condensation occur during desorption stage.

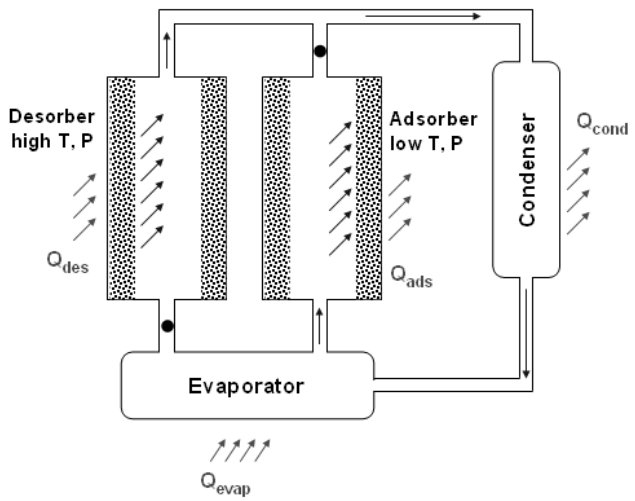

Figure 1. Simplified adsorption cooling schematic.

In the adsorption stage, liquid water is vaporized inside an evaporator at low temperature and low pressure. Cooling output of the adsorption cooling system is determined from heat supplied to the evaporator during this step. The water vapor then flows to the adsorber, which is connected to the evaporator, and is adsorbed onto the adsorbent layer. Heat is generated while water is being adsorbed on the adsorbent layer.

In the desorption stage, the adsorber becomes a desorber. Water is desorbed out of the adsorbent layer at higher temperature and pressure. Heat is consumed and needs to be supplied externally. The desorbed water vapor then flows to a condenser which is connected to the desorber. Heat is removed from the condenser as water is being condensed.

There are two key parameters used to evaluate performance of the cooling device, coefficient of performance and specific cooling power. The coefficient of performance, COP, is the ratio of the heat removed from the heat source to the energy supplied to the system, and is defined by

$$COP = \frac{|Q_{evap}|}{|Q_{des}|} \tag{1}$$

The specific cooling power, SCP, is the amount of heat that the device can remove from the heat source per time per mass of adsorbent (W/kg), and is defined by

$$SCP = \frac{|Q_{evap}|}{t_{cycle} m_{adsorbent}} \tag{2}$$

1.2 Literature Review

During the 1990s, research into the development of more efficient solid adsorption refrigeration systems was intensified, particularly in Japan, Europe and the US. [5] The three major types of studies focused on process parameter analysis, development of novel adsorbent materials, and improvement of unit operations design.

Boelman et al. [6] conducted experiments to study the influence of operating temperatures on the performance of commercialized adsorption cooling chiller. When the hot water inlet temperature was increased, the SCP increased at every operation condition. The COP increased as cooling water inlet temperature increased but COP decreased at lower cooling water inlet temperatures. Moreover, the COP increased when the temperature difference between adsorber and evaporator was reduced. A maximum COP of 0.51 was obtained.

Mass recovery and heat recovery processes have been widely embedded in adsorption cooling systems. In the mass recovery process, the desorber at high temperature and the adsorber at low temperature are opened together. This allows residual water that left in the desorber at the end of desorption stage to move to the adsorber at the end of adsorption stage. In the heat recovery process, cooling water is flowing internally between the adsorber and desorber. Therefore, heat is being transferred from the desorber to the adsorber, which improves COP.

Akahira et al. [7] included the mass recovery process to the adsorption/desorption cycle. The experiments were performed in two situations, with heating/cooling and without heating/cooling during the mass recovery process. The COP was 0.46 without heating/cooling vs. 0.36 with heating/cooling, compared to 0.36 when the mass recovery process was not included. The SCP was 120 W/kg without heating/cooling vs. 130 W/kg with heating/cooling.

Wang et al. [8] compared adsorption cooling system performance at different hot water inlet temperatures. The COP increased from 0.28 to 0.34 and the SCP increased from 63 W/kg to 135 W/kg when hot water inlet temperature was increased from 65°C to 85°C. Also, the COP was enhanced by 25% when the heat recovery process was included in the adsorption cooling process.

Kong et al. [9] studied the effect of hot water inlet temperature and chilled water inlet temperature to the performance of adsorption cooling device with mass recovery process embedded. The COP increased from 0.31 to 0.34 and the SCP increased from 49 W/kg to 90 W/kg when the hot water inlet temperature was increased from 60°C to 90°C. Increasing the chilled water inlet temperature or evaporation temperature from 15.7°C to 20.5°C improved COP from 0.26 to 0.31, and SCP from 41 W/kg to 49 W/kg.

Wang et al. [10] varied the cooling water temperature (adsorption temperature) in an adsorption cooling system that featured an embedded mass recovery process. The COP increased from 0.32 to 0.41 and cooling capacity increased from 5kW to 8.3kW when cooling water temperature was decreased from 34°C to 25°C. A maximum COP of 0.385 and cooling capacity of 4.8 kW were obtained.

Xia et al. [11] increased the performance of the device by a combination of mass and heat recovery processes, where the COP increased from 0.32 to 0.34 and the SCP increased from 50 to 81 W/kg.

Yang et al. [12] developed a compact (bench top) adsorption cooling system which had a cooling output lower than 1 kW. The COP and SCP at a hot water inlet temperature of 70°C were 0.289 and 49 W/kg, respectively. When the hot water inlet

temperature was increased to 90°C, the COP and SCP became 0.319 and 79 W/kg, respectively.

Ng et al. [13] proposed an electro-adsorption chiller, which is a combination of the adsorber and thermoelectric modules. The thermoelectric module is the device that can generate a temperature difference between two points. The COP ranged from 0.7 to 0.8 and a maximum SCP of 208 W/kg were obtained from experiment.

Beside silica gel/water as the adsorbent/adsorbate working pairs, many other adsorbent materials were developed. Daou et al. [14] impregnated silica gel with calcium chloride which improved the COP by 25% and increased the SCP by 283% compared to pure microporous silica gel. Cui et al. [15] obtained adsorption isotherm of DH-5 and DH-7 from experiments, and found that DH-5 and DH-7 adsorbed water up to 0.72 and 0.73 g water/ g adsorbent, respectively, which were far greater than silica gel and twice of the 13x molecular sieve capacity.

Wang et al. [16] reviewed new adsorbents for adsorption cooling systems. The adsorption rate was generally limited by heat transfer. The adsorbent materials were mixed with binder and appropriate conductive material before being coated on metal surface of heat exchanger. This method decreased adsorption time from 50 min to 20 min.

Yong et al. [17] summarized recent patents for cooling systems. Multi-stage adsorbers can significantly reduce the heat required for the desorption stage. Many efforts have been done to improve heat transfer rate, such coating adsorbent materials on the heat exchanger wall and embedding heat pipe in the cooling system. Developments of novel adsorbent materials that have high adsorption capacity were also mentioned.

The COP, SCP and important operating parameters from previous studies are summarized in Table 2. All previous work used hot water to carry out the desorption stage because the adsorption cooling system was originally designed to utilize waste heat generated from chemical plants, which is typically in the form of hot water at temperature below 100°C. Most researchers showed that the COP increased when the hot water inlet temperature was increased, with the exception of Boelman's work[6].

Boelman showed that the COP decreased when hot water inlet temperature was increased at operating conditions shown in Table 2. All previous studies confirmed that SCP increases when the hot water inlet temperature was increased.

Table 2. Summary of previous studies on adsorption cooling.

Reference	Process Description				Operating Temperature**			Process Performance	
	Configuration	Method of Desorption	Adsorbent	Working Fluid	T_{evap} (^oC)	T_{ads} (^oC)	T_{des} (^oC)	COP	SCP (W/kg)
Boelman et al. [6]	packed-bed, single-stage	hot water	silica gel	water	14-16	25	70	0.51	14.16 kW*
					14-16	20	50	0.48	10.40 kW*
					14-16	20	70	0.43	14.86 kW*
					14-16	20	85	0.34	15.99 kW*
Akahira et al. [7]	packed-bed, single-stage	hot water	silica gel	water	7-14	30	80	0.4	85
					7-14	30	70	0.36	56
					7-14	30	60	0.12	11
	packed-bed, single-stage, mass recovery	hot water	silica gel	water	7-14	30	70	0.46	62
Wang et al. [8]	packed-bed, single-stage	hot water	silica gel	water	8-12	29.4	65	0.28	63
					8-12	29.4	85	0.34	135
Kong et al. [9]	packed-bed, single-stage, mass recovery	hot water	silica gel	water	16-20	30.6	90	0.34	90
					16-20	30.6	75	0.33	73
					16-20	30.6	60	0.31	49
					12-16	30.6	60	0.26	41
Wang et al. [10]	packed-bed, single-stage, mass recovery	hot water	silica gel	water	18-20	30.4	59.7	0.385	4.8 kW*
					18-20	25	65.4	0.41	8.3 kW*
Xia et al. [11]	packed-bed, single-stage	hot water	silica gel	water	12-16	31	85	0.32	50
					12-16	31	75	0.32	43
					12-16	31	65	0.28	29
	packed-bed, single-stage, mass-heat recovery	hot water	silica gel	water	12-16	31	85	0.34	81
					16-20	31	85	0.404	100

* Amount of adsorbent was not indicated. Cooling output was reported instead of SCP.

** T_{evap}, T_{ads} and T_{des} are evaporator temperature, adsorption temperature and desorption temperature, respectively.

Table 2. Summary of previous studies on adsorption cooling (Continued).

Reference	Process Description				Operating Temperature**			Process Performance	
	Configuration	Method of Desorption	Adsorbent	Working Fluid	T_{evap} (^oC)	T_{ads} (^oC)	T_{des} (^oC)	COP	SCP (W/kg)
Yang et al. [12]	packed-bed, single-stage	hot water	silica gel	water	16-20	28	90	0.319	79.22
					16-20	28	80	0.319	68.01
					16-20	28	70	0.289	48.93
Ng et al. [13]	packed-bed, single-stage	thermoelectric	silica gel	water	20	35	75	0.7-0.8	208
Daou et al. [14]	packed-bed, single-stage	hot water	silica gel	water	10	30	70	0.265	25
		hot water	$CaCl_2$-impregnated silica gel	water	10	30	70	0.331	55

** T_{evap}, T_{ads} and T_{des} are evaporator temperature, adsorption temperature and desorption temperature, respectively.

The major advantages of microchannel devices include rapid heat and mass transfer, precise control of process conditions, low inventory of hazardous reactions, use of surface phenomena to significant advantage, and overall process intensification [18]. Harpole et al. [19] developed a model for microchannel heat exchanger and found that the effective heat transfer coefficient on the order of 100 W/cm^2-K can be achieved for mixture of water and methanol as the working fluid. Wang et al. [20] developed a microchannel heat exchanger for integrated circuit (IC) cooling application and reported that the calculated Nusselt number (Nu) was larger than for macroscopic channels. Also, a maximum heat transfer coefficient of 14712 W/m^2-K was obtained for water as the working fluid. Brandner et al. [21] fabricated several sizes of microchannel heat exchangers and found that the heat transfer in microstructured heat exchangers can be enhanced by decreasing the hydraulic diameter of microchannels from 144 to 70 μm. Jiang et al. [22] studied heat transfer characteristics of rectangular microchannels. The Nusselt number (Nu) increased with the increase in the Reynolds number. When the flow became turbulent, Nu exceeded the value predicted by conventional correlations.

Most of the previous work on heat transfer in microchannels reported that the Nusselt number (Nu) is increased when the flow channels dimensions are minimized to microscale. Therefore, the convective heat transfer coefficient (h) is significantly enhanced in the microchannel heat exchanger devices.

1.3 Goals and Objectives

The adsorption cooling process is well studied and microchannel technology is widely known for its intensification of heat transfer. However, there are no studies showing how microchannel technology can be used for improving heat transfer in adsorption cooling applications.

The goal for this research is to develop a microtechnology-based adsorption device for adsorption cooling application using water as working fluid and silica based material as adsorbent.

To achieve the research goal, there are two objectives.

1. Fabricate the microtechnology-based adsorption device;
2. Evaluate the performance of the finished device and determine the optimum operating parameters for the adsorption/desorption cooling cycle.

Chapter 2 - Materials and Methods

2.1 Microchannel Adsorption Device Fabrication

The basic microchannel architecture is described in Figure 2. The air flow channels are used to drive heat transfer to the adsorption channels. Fluid flow in the air flow channels is isolated from the adsorption channels. The air flow channels operate at atmospheric pressure or higher, while the adsorption channels must be kept under partial vacuum during the operation. Aluminum is used as the housing metal because of its high thermal conductivity (237 W/m-K at 300 K)[23] and low density (2.55-2.80 g/cm^3)[23]. Because aluminum continuously forms its native oxide film on the surface when exposed to oxygen, the diffusion bonding technique cannot use to bond these aluminum shims together. Therefore, B-staged epoxy adhesive thin film was chosen for bonding. The epoxy has curing temperature of 120-150°C the cured device can be operated at temperature up to 200°C without deteriorating the adhesion of the epoxy to the metal.

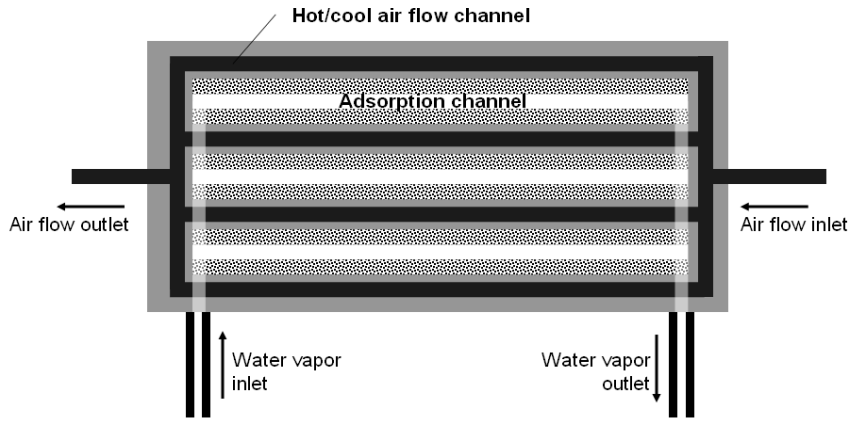

Figure 2. Simplified cross-sectional schematic of microchannel adsorption device.

The three major components used to fabricate the microchannel adsorption device are aluminum shims, silica gel plates and adhesive thin films. There are 5 different types of 2.0 inch x 2.0 inch aluminum shims, Type 1-5. Type 1 and Type 2 aluminum shims, is the 450 μm-thick aluminum sheet cut to 2.0 inch x 2.0 inch. The

Type 1 shim is used as the bottom plates while the Type 2 shim is for the top plate. In addition, two holes are drilled on the Type 2 shim to serve as inlet and outlet ports for the adsorption channels. The Type 3 aluminum shim is a solid separator between air flow and adsorbent channels. The Type 4 aluminum shim is flow channel for both adsorbent and air layers. Each of Type 4 aluminum shim divides flow from the header into six identical sub-channels. Each sub-channel has 5.7 mm width, 400 μm height and 4.7 cm length. The Type 5 aluminum shim is a gasket for the adsorbent layer. The Type 5 shim is located on the same layer as the silica gel plate adsorbent layer. The Type 3-5 shims have identical thickness of 400 μm. Schematic of all types of aluminum shims and the silica gel plate are shown in Figure 3. The Type 1 and Type 2 shims were cut by a sheer cutter. The Type 3-5 shims were cut using wire electrical discharge machining (EDM) at Wright Prototype, Inc. (Albany, Oregon). The Type 1-5 shims weigh 3.186 g, 3.186 g, 2.528 g, 0.906 g and 0.652 g, respectively.

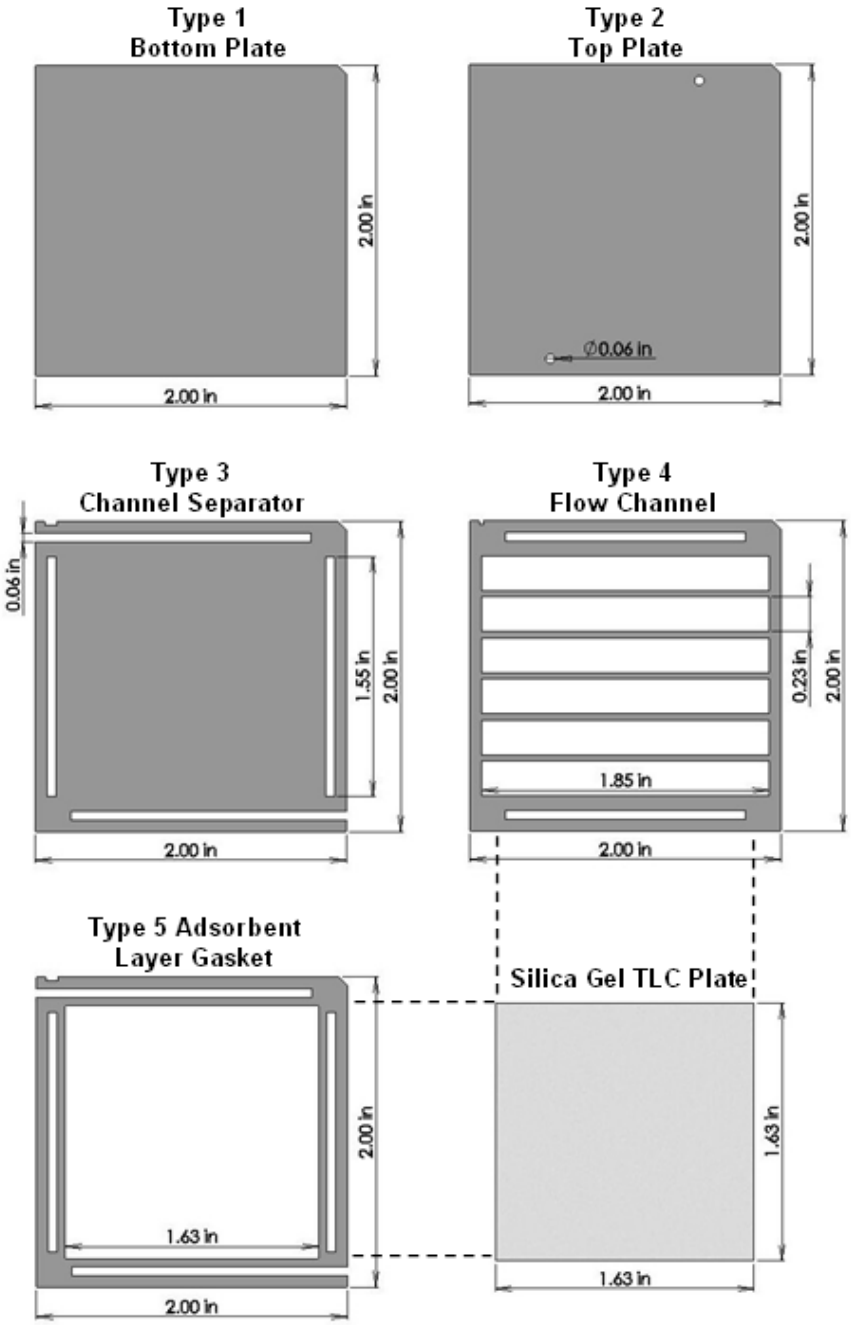

Figure 3. Drawings of aluminum shims and silica gel TLC plate.

Silica gel thin TLC plates were purchased from Whatman plc. Each TLC sheet has original dimensions of 20 cm x 20 cm. They were cut to several plates of 1.63 inch x 1.63 inch with a 355 nm laser (ESI model 5330 UN Laser µvia Drill). A schematic

of the cut silica gel plate is shown in Figure 3, while the actual picture is shown in Figure 4. Each silica gel plate weighs 0.657 g, 0.165 g from silica gel and 0.492 g from the aluminum support.

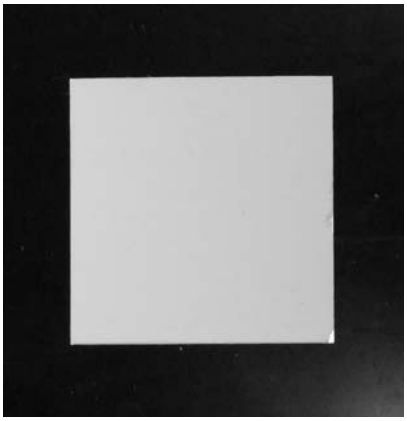

Figure 4. Silica gel TLC plate.

The epoxy adhesive thin films were obtained from TechFilm Service Inc., Billerica, MA (TF T2222F). They originally came in 8 inch x 8 inch sheet with thickness of 0.002 inch (50 μm) over a wax paper liner. The adhesive films were then cut into two patterns with the 355 nm laser. Pattern 1 and 2 adhesive films are shown in Figure 5. Pattern 1 adhesive film was applied on the Type 3 separator shim but only to the side that faces the silica gel plate. Pattern 2 adhesive films were placed on top of all other shims.

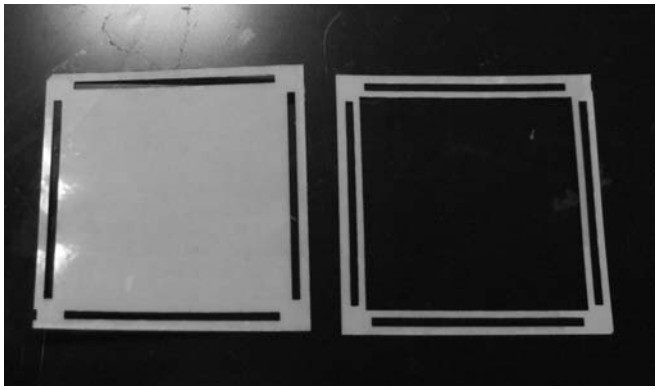

Figure 5. Pattern 1 (left) and pattern 2 (right) adhesive films.

An exploded-view schematic of single layer microchannel adsorption device, including epoxy thin film layers, is shown Figure 6a. The single-layer device consists of one adsorption channels layer and two air flow channels layers. The purpose of air flow channels is to transfer heat to and from the adsorption channel. One air flow channels layer is located above while another one is below the adsorption channels layer. In addition, the air flow channels layers and adsorption channels layers are completely isolated. The air flow direction is perpendicular to that of adsorption channel. (See Figure 7a) The repeat unit, shown in Figure 6b, can be added to increase number of adsorption channels (or layers). In this research, single-layer and three-layer microchannel adsorption devices were fabricated. The design and summary of both single-layer and three-layer device is presented in Table 3. The assembled drawing of the single-layer device including inlets and outlets is shown in Figure 7b, and the cross-sectional isometric views for the single-layer and three-layer device are shown in Figure 7c and 7d, respectively.

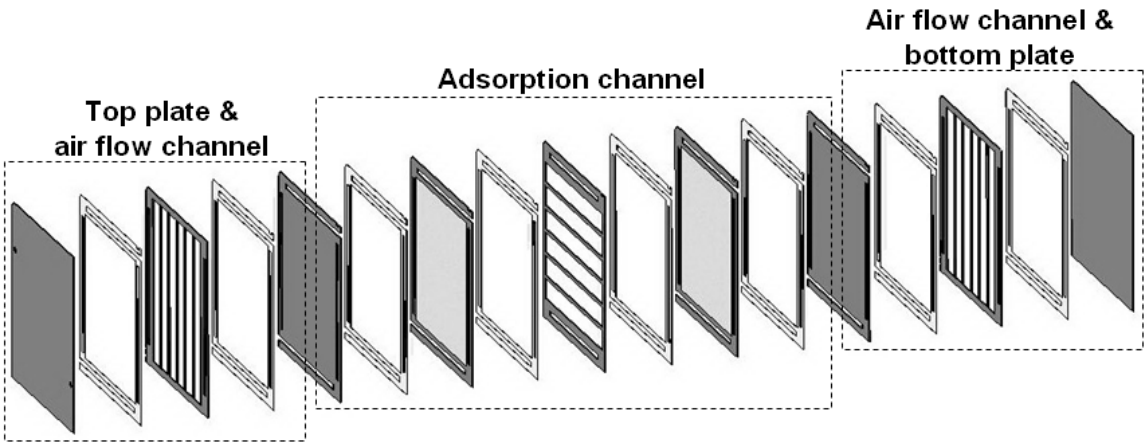

(a)

Figure 6. Exploded drawing of a single-layer microchannel adsorption device featuring (a) air flow channels and adsorption channel, (b) repeat unit.

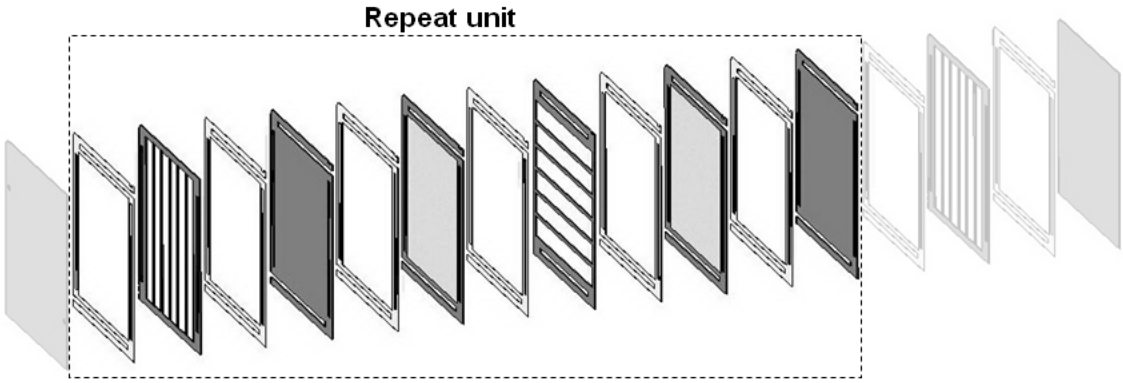

(b)

Figure 6. Exploded drawing of a single-layer microchannel adsorption device featuring (a) air flow channels and adsorption channel, (b) repeat unit. (Continued)

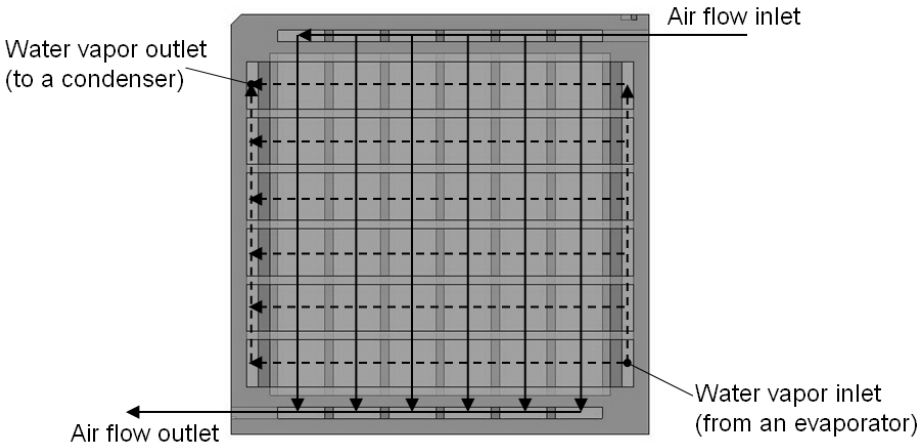

(a)

Figure 7. Schematics of assembled device with flow directions. (a) Top-view, (b) isometric view, (c) single-layer, cross-sectional isometric view, and (d) three-layer, cross-sectional isometric view.

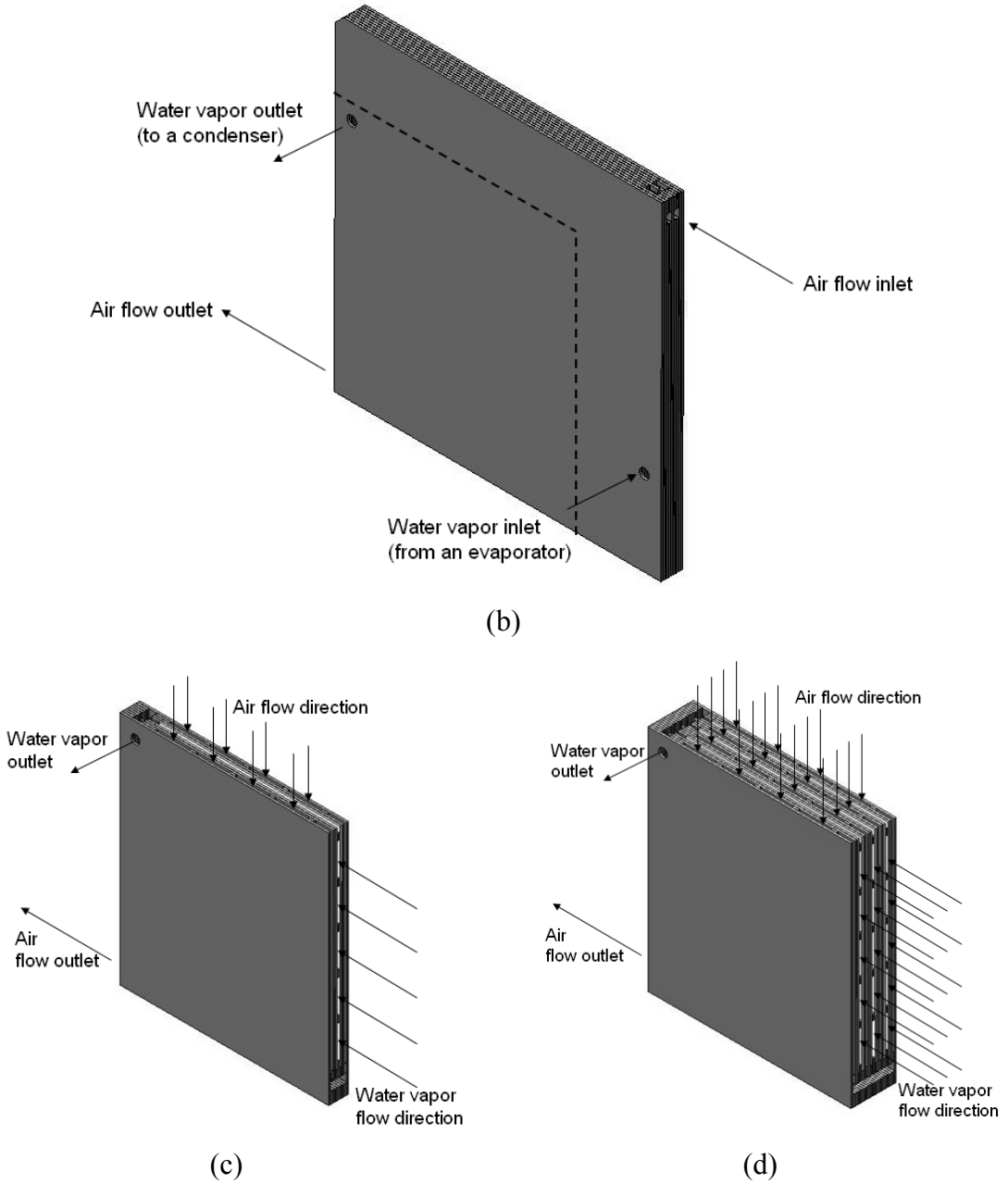

Figure 7. Schematics of assembled device with flow directions. (a) Top-view, (b) isometric view, (c) single-layer, cross-sectional isometric view, and (d) three-layer, cross-sectional isometric view. (Continued)

Table 3. Summary of the fabrication parameters for the single-layer and three-layer microchannel adsorption device.

Device feature	Value and units	
	Single-layer device	Three-layer device
Total adsorbent weight	0.329 g	0.988 g
Total aluminum weight	21.382 g	39.694 g
Total mass (fittings excluded)	21.711 g	40.682 g
Aluminum/adsorbent mass ratio	64.8	40.1
Number of air flow channels	2	4
Number of adsorption channels	1	3
Outer dimension (W x L)	5.1 x 5.1 cm	5.1 x 5.1 cm
Active dimension (W x L)	4.6 x 4.6 cm	4.6 x 4.6 cm
Shim stack thick ness	4.4 mm	10.2 mm

To make the three-layer microchannel adsorption device, 21 aluminum shims, 40 adhesive thin films and 6 silica gel TLC plates were required. The stacking sequence is shown in Table 4. All aluminum shims were cleaned in mixture of 1:1 acetone and methanol under sonication at room temperature for 10 min. The wet shims were then dried in air. After drying, each adhesive thin film was transferred from a wax paper liner to one side of aluminum shim surface. Prior to adhesive application, the aluminum shim was pre-heated to 70-90°C by an electrical hot plate. The adhesive thin film (at room temperature) was aligned and pressed to the warm aluminum shim. Then, another adhesive film was transferred to another side of the same aluminum shim. Most of aluminum shims required the Pattern 2 adhesive film, except the Type 3 shim, which required the Pattern 1 film on the side facing to TLC plate. After both sides of all shims were covered with adhesive films with wax paper liners intact, shims were pre-stacked on a fixture to ensure the correct alignment as shown in Figure 8. Then wax paper liners were all peeled off from aluminum shims. Boron nitride aerosol was sprayed onto the fixture to prevent sticking between the fixture and a bonded device. Aluminum shims were stacked onto the bottom part of fixture, starting with the Type 1 shim. After all shims and TLC plates were aligned, the top part of fixture was placed above the shim array. The whole assembly was clamped and put into the furnace at 120°C. The device was bonded together after 2 hr adhesive curing time in the furnace. The bonded microchannel devices, single-layer and three-layer, are shown

in Figure 9. After that, the inlet and outlet ports were attached to the device using J-B Weld glue. J-B Weld glue was chosen instead of metal soldering because metal soldering requires high temperature that cand damage the adhesive film layer and TLC plate. Moreover, the J-B Weld glue requires longer setting time, so the viscous glue can slightly flow and fill all the air gaps. The completed microchannel adsorption device is shown in Figure 10.

Table 4. Aluminum shim stacking sequence.

Top	Type 1 aluminum shim (2 holes drilled)
	Type 4 shim, flow channel (90° rotated)
	Type 3 shim, separator
	Type 5 shim, gasket / silica gel TLC plate (faced down)
	Type 4 shim, flow channel
	Type 5 shim, gasket / silica gel TLC plate (faced up)
	Type 3 shim, separator
	Type 4 shim, flow channel (90° rotated)
	Type 3 shim, separator
	Type 5 shim, gasket / silica gel TLC plate (faced down)
	Type 4 shim, flow channel
	Type 5 shim, gasket / silica gel TLC plate (faced up)
	Type 3 shim, separator
	Type 4 shim, flow channel (90° rotated)
	Type 3 shim, separator
	Type 5 shim, gasket / silica gel TLC plate (faced down)
	Type 4 shim, flow channel
	Type 5 shim, gasket / silica gel TLC plate (faced up)
	Type 3 shim, separator
	Type 4 shim, flow channel (90° rotated)
Bottom	Type 1 shim, bottom plate

(a)

(b)

Figure 8. Fixture, (a) bare, and (b) clamped.

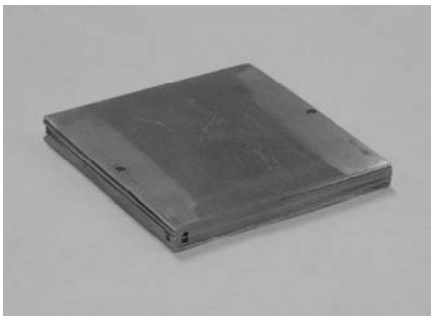

(a)

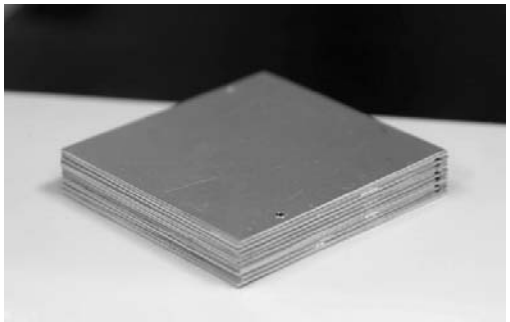

(b)

Figure 9. Bonded microchannel adsorption device, (a) single-layer, and (b) three-layer.

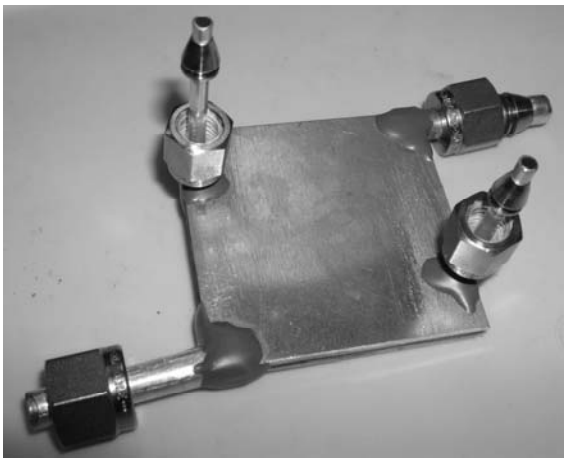

Figure 10. Completed microchannel adsorption device.

Since the adhesive thin film is placed between the silica gel TLC plate and the aluminum separation plate, there will be additional heat transfer resistance from this thin film layer. The thermal conductivity of the adhesive thin film is 0.75 W/m-K, which is considered significantly higher than that of air (0.025 W/m-K) but still way lower than that of aluminum (237 W/m-K). The heat transfer across each layer is presented in Figure 11.

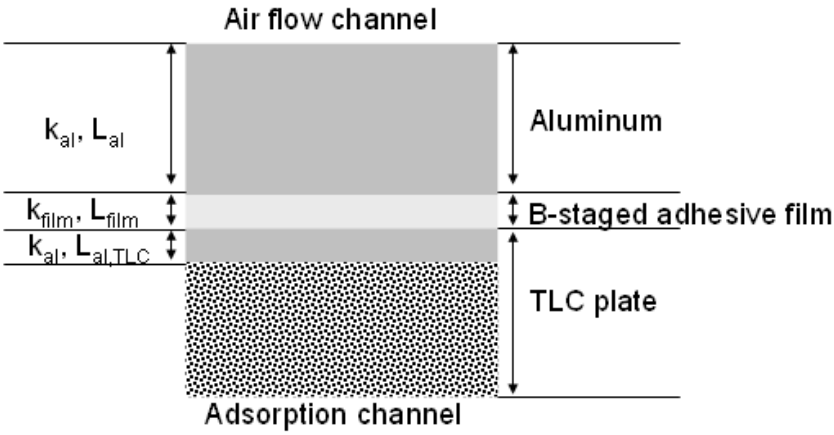

Figure 11. Schematic of heat transfer resistance between air flow channel and adsorption channel.

The total resistance, R_{total}, is defined by equation (3).

$$R_{total} = \frac{1}{A}\sum_i \frac{L_i}{k_i} \qquad (3)$$

where A is an area of heat transfer (m^2), L_i is thickness of each layer (m) and k_i is thermal conductivity of each layer (W/m-K).

Thickness and thermal conductivity of each layer are presented in Table 5. The calculated (L/k) values are 1.7 x 10^{-6} m^2-K/W, 6.7 x 10^{-5} m^2-K/W and 1.1 x 10^{-7} m^2-K/W for separation aluminum plate, B-staged adhesive thin film and aluminum support of TLC plate, respectively. The adhesive film seems to offer the highest resistance.

Table 5. Thermal conductivity and thickness of each layer between air flow channel and adsorbent layer

Layer	Thickness, L (μm)	Thermal conductivity, k (W/m-K)
Type 3 separation aluminum shim	400	237
B-stages adhesive film	50	0.75
Aluminum support of silica gel plate	25	237

2.2 Water Adsorption Isotherm on Silica Gel

Silica gel can adsorb different amounts of water when temperature and pressure of water vapor changes.

Silica gel thin layer chromatography (TLC) plates were obtained from Whatman plc. The average thickness of silica gel layer is 250 μm while aluminum back support is 25 μm thick. The pores within the silica gel particles have average diameter of 60Å. (Catalog number 4420-222)

The experiments for obtaining adsorption isotherm were separated into two parts. In experiment 1, the TLC plate was exposed to saturated water vapor. In experiment 2, the TLC plate was exposed to superheated water vapor.

In experiment 1, the silica gel TLC plate (2.5 cm x 3.0 cm) was placed inside a closed 250 mL container that contained 10 mL of liquid water. The TLC plate did not contact the liquid water and was then exposed to saturated water vapor. The closed container was then placed in a temperature controlled temperature incubator for 2 hr to ensure that the vapor phase was saturated with water and that the water uptake on silica gel has reached equilibrium. Then, the weight of the TLC plate was measured and then normalized to water uptake (g water/ g silica gel). The experiment was repeated at different temperatures ranging from 11°C to 80°C.

In experiment 2, the saturated water vapor was generated by bubbling air through series of two 250 mL flasks containing 200 mL of water at 24°C. Air with partial pressure water of 22.38 torr was then heated up to high temperature, so the water-saturated air was changed to the superheated state. After that, air flowed through adsorption channels of the three-layer microchannel device which was placed inside the temperature controlled temperature incubator. The device was weighed after 1 hr to ensure the equilibrium has been reached. The experiment was then repeated at different temperature ranging from 30°C to 80°C.

2.3 Water Adsorption Rate

The microchannel device was exposed to water vapor at constant temperature and pressure for a specific time. To ensure constant temperature, air at the adsorption temperature continuously flew through the air flowed channels of the device. The device was weighed and the water uptake was calculated. The experiment was then repeated at a different time. The adsorption rate constant (k) and equilibrium water uptake (L^*) at specific temperature were then obtained from experimental results.

2.4 Test Loop Configuration

The test loop schematic is shown in Figure 12. There were five thermocouples and two pressure transducers connected to a National Instrument data acquisition system. Thermocouples (Omega, Type K) were used to measure temperatures at the air flow inlet (T_1), the air flow outlet (T_2), microchannel device wall (T_3), inside the evaporator (T_4) and inside the condenser (T_5) while the pressures were measured inside the adsorber (P_1) and at the flow meter (Matheson Tri-Gas, 604) downstream (P_2). The evaporator was separated from a microchannel adsorption device by valve V1 while the condenser was separated from the device by valve V2b. Valve V4 and V5 were used to fill an evaporator and a condenser, respectively, with water to a desired level. Either valve V2a or V3 could be connected to the vacuum pump for system air removal.

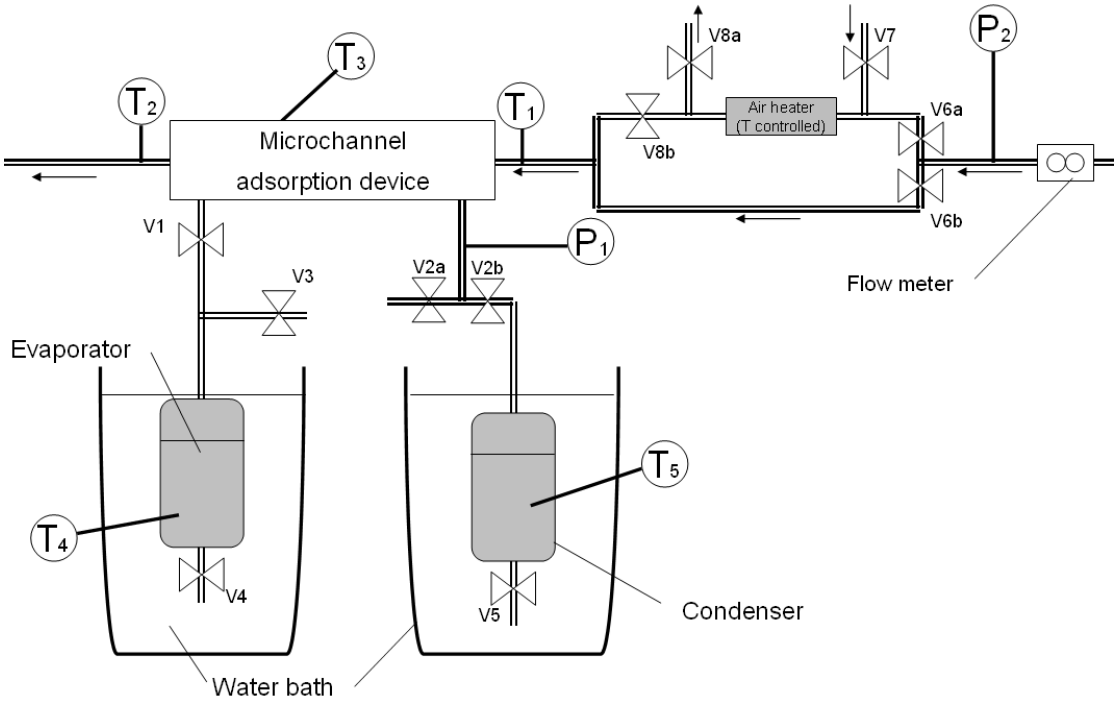

Figure 12. Test loop schematic.

2.5 Adsorption/Desorption Cycle

A single adsorption/desorption cycle could be divided into 4 steps which were: (1) isolated adsorption, (2) active adsorption, (3) isolated desorption, and (4) active desorption. The valve configuration during each step is shown in Table 6.

Table 6. Valve configuration for the test loop

Valve	Step 1	2	3	4
V1	closed	open	closed	closed
V2a	closed	closed	closed	closed
V2b	closed	closed	closed	open
V3	closed	closed	closed	closed
V4	closed	closed	closed	closed
V5	closed	closed	closed	closed
V6a	closed	closed	open	open
V6b	open	open	closed	closed
V7	open	open	closed	closed
V8a	open	open	closed	closed
V8b	closed	closed	open	open

Note -V2a and V2b are combined to V2 three-way valve, as well as V6 and V8.

During Step 1, isolated adsorption, the adsorption channels of the microchannel device were isolated from both evaporator and condenser. The residual water vapor in the vapor phase was adsorbed back into the silica gel layers while the device was being cooled by air flowing through the air flow channels. The isolated adsorption step ended when the pressure of the device was equal to the pressure of the evaporator.

Step 2 was active adsorption. The adsorption channels were opened to the evaporator while the whole device was maintained at low temperature. Water vapor that evaporated from the evaporator flowed into the adsorption channels and was adsorbed onto the silica gel layers. The majority of water adsorption occurred during this step. The amount of water adsorbed in this step reflected the amount of heat that was removed from the heat source (evaporator) in one cycle.

After water is adsorbed, Step 3, isolated desorption, began. The adsorber was again isolated from the evaporator and the condenser. The device was heated up by hot air. Small amount of water was desorbed out of silica gel layers. This step ended when the pressure reached the pressure of the condenser.

Step 4 is active desorption. The device was still kept at high temperature. The adsorber was connected to the condenser so that water desorbed out of the device could flow to the condenser and condense there. The majority of desorption occurred during this step.

Chapter 3 – Results and Discussion

3.1 Adsorption Isotherm

The adsorption isotherm of water on silica gel TLC plate is presented in Figure 13. The experimental results include equilibrium water uptake when the silica gel was exposed to saturated water vapor at operating temperatures, and when it was exposed to water vapor at a partial pressure of 22.38 torr. The equilibrium water uptake decreased when temperature increased at both pressure conditions. At the same temperature, the equilibrium water uptake decreased when lower partial pressure of water was supplied. The solid curves in Figure 13 represent data fitted into an equation (4) form[24]. All fitted coefficients are shown in Table 7.

$$L^* = A\left(\frac{P}{Psat}\right)^B \tag{4}$$

where A and B are functions of temperature, T, in Kelvin.

$$A = A_0 + A_1 \cdot T + A_2 \cdot T^2 + A_3 \cdot T^3$$

$$B = B_0 + B_1 \cdot T + B_2 \cdot T^2 + B_3 \cdot T^3$$

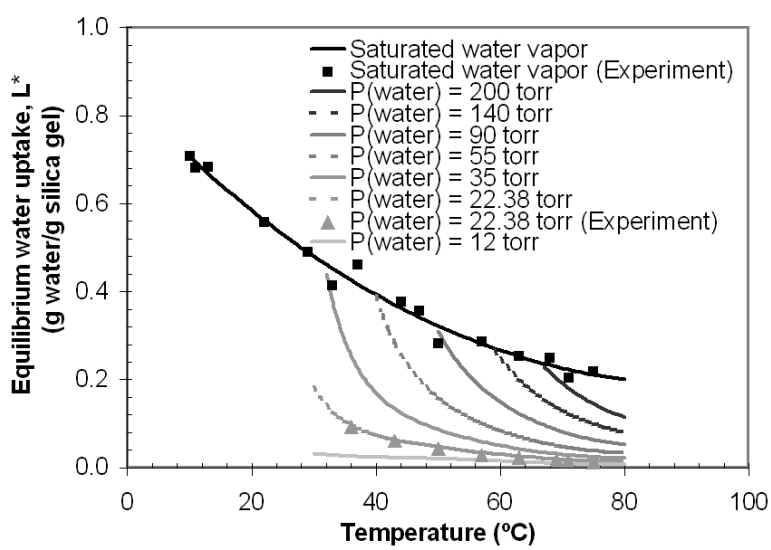

Figure 13. Adsorption isotherm of water on silica gel TLC plate.

Table 7. Coefficients for the empirical adsorption isotherm of water vapor on silica gel.

Coefficient	Value
A_0	1.396×10^{1}
A_1	-8.876×10^{-2}
A_2	1.771×10^{-4}
A_3	-1.022×10^{-7}
B_0	$1.010E \times 10^{3}$
B_1	-8.850
B_2	2.590×10^{-2}
B_3	-2.528×10^{-5}

3.2 Water Adsorption Rate in the Microchannel Adsorption Device

Profiles of water uptake onto the three-layer microchannel adsorption device at three constant temperatures are presented in Figure 14. During the experiment, the temperature of an evaporator was maintained at the same temperature of a microchannel device. This ensured that a microchannel device was exposed to saturated (or almost saturated) water vapor at the device operating temperature. At lower temperatures, the microchannel device adsorbed more water but it took longer time to reach the equilibrium extent of water vapor adsorption. The extent of water sorption on the silica gel with time is given by [25]

$$L(t) = L^{*} \cdot \left(1 - e^{-kt}\right) \qquad (5)$$

where L^{*} is an equilibrium extent of water vapor adsorption (g water/g silica gel) at specific temperature and partial pressure of water and k is an adsorption rate constant which is a function of temperature. The solid lines in Figure 14 represent data that were fitted to the equation (5) using a non-linear least squares method. The adsorption rate constants (k) and equilibrium extents of water vapor adsorption (L^{*}) are compared in Figure 15. The adsorption rate constant decreased when temperature was lowered, which means that the adsorption was taking longer at lower temperatures.

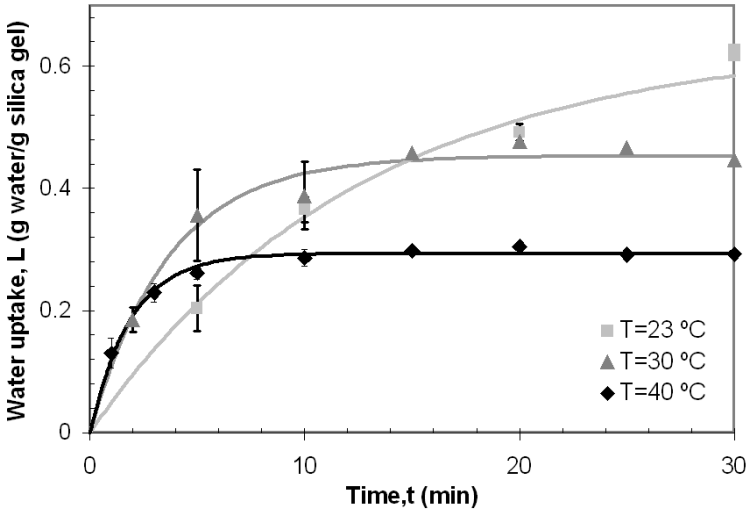

Figure 14. Water uptake on silica gel TLC plate in the three-layer microchannel device.

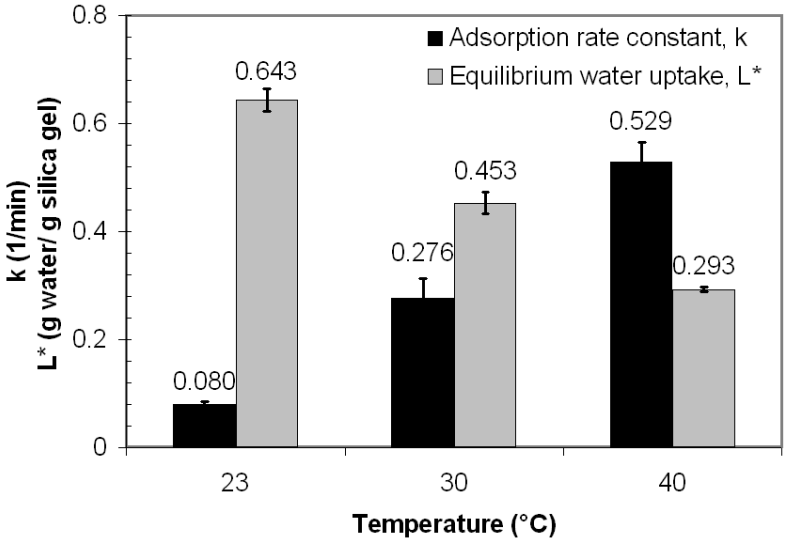

Figure 15. Comparison of water adsorption rate constant and equilibrium water uptake at temperatures of 23°C to 40°C.

3.3 Adsorption/Desorption Cycle of the Single-Layer Microchannel Adsorption Device

Pressure and temperatures profiles of four consecutive adsorption/desorption cycles are shown in Figure 16a. Figure 16b presents pressure, temperature, temperature derivative ($\frac{dT_3}{dt}$) profiles for the second adsorption/desorption cycle. Figure 17 presents the pressure-temperature diagram of two consecutive adsorption/desorption cycles.

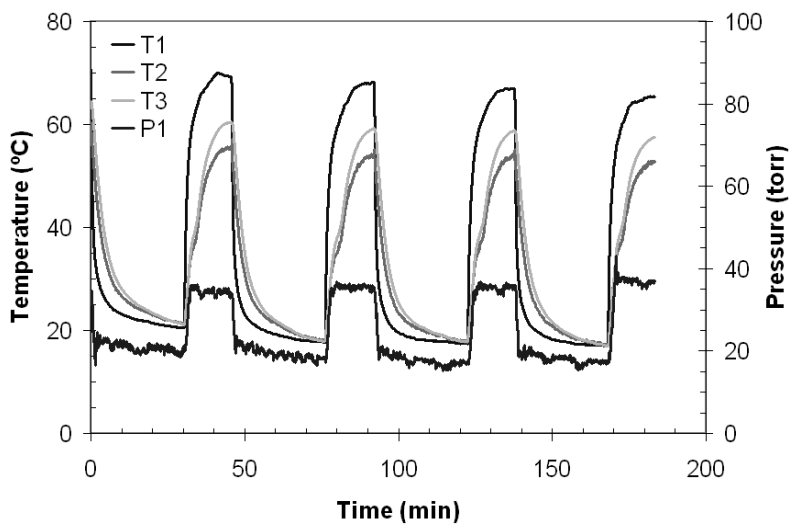

(a)

Figure 16. Pressure and temperatures profiles for adsorption/desorption cycle of single-layer microchannel adsorption device. (a) Four consecutive adsorption/desorption cycles and (b) detail of the second adsorption/desorption cycle.

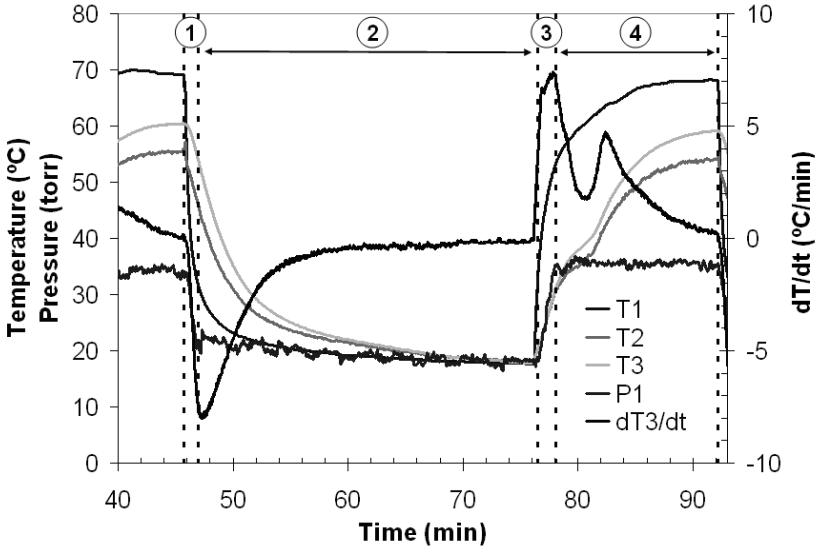

(b)

Figure 16. Pressure and temperatures profiles for adsorption/desorption cycle of single-layer microchannel adsorption device. (a) Four consecutive adsorption/desorption cycles and (b) detail of the second adsorption/desorption cycle. (Continued)

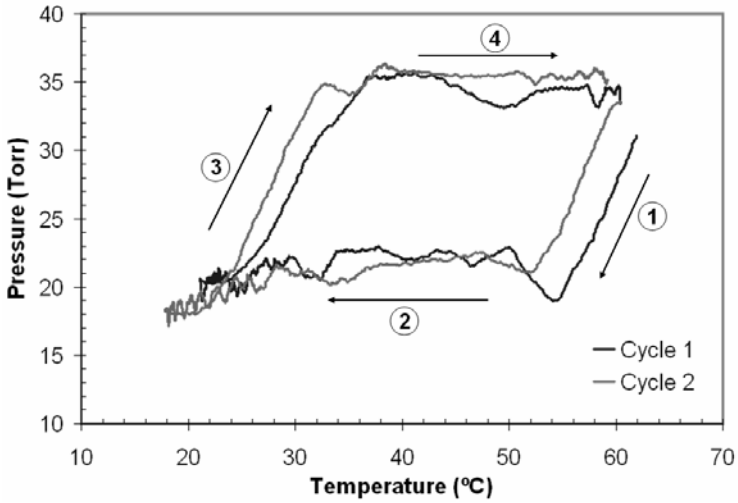

Figure 17. Pressure-temperature diagram for two successive adsorption/desorption cycles in the single-layer microchannel adsorption device.

During Step 1 (isolated adsorption), the air inlet temperature (T_1) quickly decreased because the hot air flow in the air flow channels is switched over to the cool

air flow. The air outlet and device surface temperatures, T_2 and T_3, responded more slowly because heat needed to be removed from the device. The pressure inside the adsorption channels decreased because temperature decreased as the water in the vapor phase was adsorbed into silica gel layers. Step 1 ended when pressure was down to the evaporator pressure. This step took only 1.5 min based on the operating parameters shown in Table 8.

During Step 2 (active adsorption), water vapor from the evaporator was adsorbed onto the silica gel layers. The majority of adsorption occurred during this step. At the starting point of this step, the device is still at a moderate temperature of 50-55°C. However, the temperature decreased at slower rate than Step 1 because the adsorption of water released heat at the same time and the temperature difference between the device and cool air flow was getting lower. The pressure inside the device was constant because it was controlled by the temperature of the evaporator. Step 2 ended when specific time of 30 min elapsed. Amount of water transferred during Step 2 was then used estimate the cooling output of the device, Q_{evap}, given by

$$Q_{evap} = m_{evap} \Delta H_{evap} \tag{6}$$

where m_{evap} is the amount of water evaporated from an evaporator in one adsorption cycle (J), and ΔH_{evap} is the specific heat of evaporation (ΔH_{evap}=2450 J/g at 22°C)[26].

Step 3 is isolated desorption process. The temperature of the device (T_3) increased rapidly because hot air flowed through the air flow channels. The pressure also increased because the device temperature (T_3) increased and water was desorbed to the vapor phase. This step took about 2 min. Only small amount of water was desorbed in Step 3.

Step 4 in single adsorption/desorption cycle is active desorption. The temperature of the device (T_3) increased slower than Step 3 because the majority of desorption occurred during this period. The device temperature increased again after

most of water was desorbed. The active desorption step was completed when the temperature of the device became constant.

Table 8. Process input and output parameters for the single-layer microchannel adsorption cooling device.

Process parameter	Value and unit
Process input	
Evaporator	
Temperature, T_{evap}	22 ºC
Pressure	19.8 torr
Condenser	
Temperature, T_{cond}	30 ºC
Pressure	31.8 torr
Dimensions of air flow channel	
Height	400 µm
Width	8.5 mm
Hydraulic diameter, D_h	760 µm
Length	4.4 cm
Air channel inlet temperature	
Adsorption stage	23 ºC
Desorption stage	70 ºC
Air channel flow rate	6.98 SLPM, 8.65 g/min
Air channel inlet pressure	500 torr (gauge)
Velocity of air in each channel	2.7 m/s at 25°C and atmospheric pressure
Calculated convective heat transfer coefficient, h	73.4 W/m^2-K
Cycle time	
Adsorption stage, t_{ads}	30 min
Desorption stage, t_{des}	15 min
Process output	
Water sorption	
Adsorption stage (final)	0.455 ± 0.120 g water/ g silica gel
Desorption stage (final)	0.027 ± 0.009 g water/ g silica gel
Cooling output, Q_{evap}	346 ± 92 J
Heat input for desorption, Q_{des}	2340 ± 97 J
Coefficient of performance, COP	0.148 ± 0.039
Specific cooling power, SCP	389 ± 103 W/kg silica gel

As mentioned previously, the coefficient of performance (COP) and the specific cooling power (SCP) are two important parameters used to evaluate the cooling device performance. COP and SCP are defined by

$$COP = \frac{|Q_{evap}|}{|Q_{des}|} \tag{1}$$

$$SCP = \frac{|Q_{evap}|}{t_{cycle} m_{adsorbent}} \tag{2}$$

The total amount of heat supplied to the device during the desorption stage (Step 3 and 4) is defined as Q_{des}, which is estimated by

$$Q_{des} = \oint_{Des} \dot{m}_{air} C_{p,air} (T_1 - T_2) dt \tag{7}$$

where $\dot{m}_{air}$ is the mass flow rate of air (g/min), $C_{p,air}$ is the specific heat capacity of air (J/g-K), T_1 or T_{in} is the temperature at the inlet of air flow channel (K), T_2 or T_{out} is the temperature at the outlet of air flow channel (K). Values for $\dot{m}_{air}$ can be estimated by

$$\dot{m}_{air} = \dot{Q}_{air,std} \rho_{air,std} \tag{8}$$

where $\dot{Q}_{air,std}$ is standard volumetric flow rate of air (SLPM), and $\rho_{air,std}$ is air density at the standard condition (g/L). Each value of $\dot{Q}_{air,std}$ is obtained from a calibration chart of the flow meter at a specific in-line pressure. [28] The calibration chart is located in Appendix C. The velocity of air in each microchannel (v_∞) is calculated by

$$v_\infty = \frac{\dot{Q}_{air,std}}{n_{air\ channel} A_{cross}} \tag{9}$$

where $n_{air\ channel}$ is a number of air flow channels in the device, and A_{cross} is a cross-sectional area of each microchannel (m^2). Figure 18 shows temperature profiles and cumulative heat transferred to the device. The average Q_{des} values are presented in Table 8.

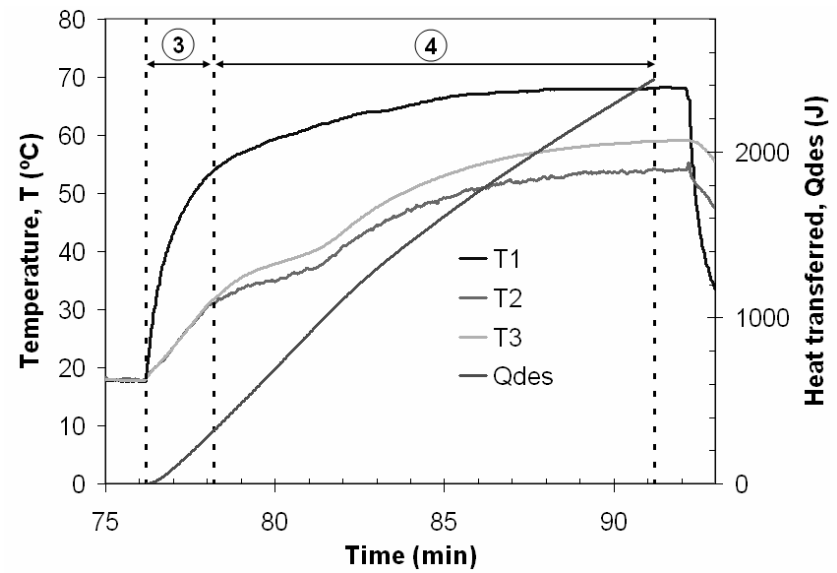

Figure 18. Temperature profiles and cumulative heat transferred to the single-layer microchannel adsorption device during the second adsorption/desorption cycle.

3.4 Adsorption/Desorption Cycle of the Three-Layer Microchannel Adsorption Device

Pressure and temperature profiles during adsorption/desorption cycle of the three-layer microchannel adsorption device are presented in Figure 19. Figure 19a shows the profiles of three consecutive adsorption/desorption cycles. Figure 19b presents detail for the third adsorption/desorption cycle. The pressure-temperature diagram is presented in Figure 20. The operating parameters for Base Case and the calculated performance are shown in Table 9. The pressure and temperature profiles were quite similar to those of the single-layer device because the temperature was

controlled by the same method and pressures during Step 2 and 4 were controlled by the temperatures inside the same evaporator and condenser.

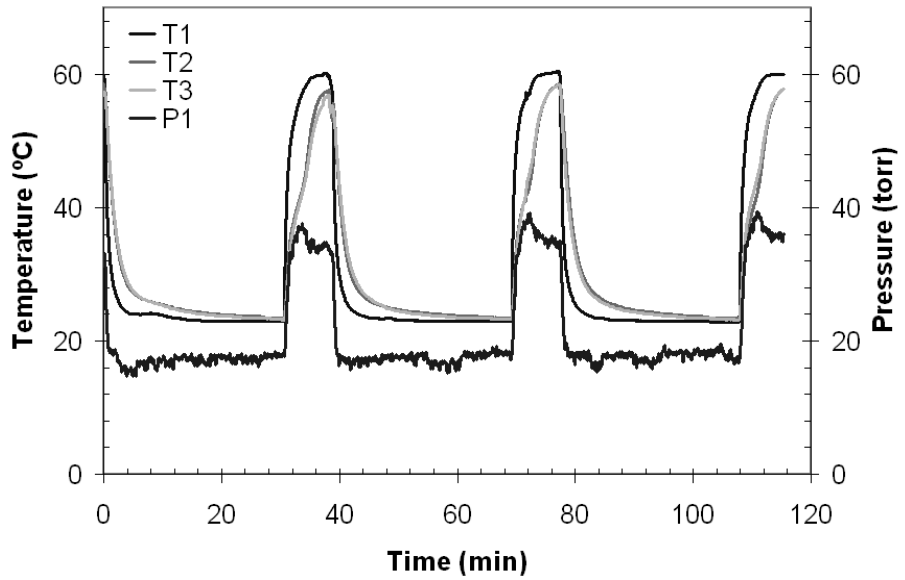

(a)

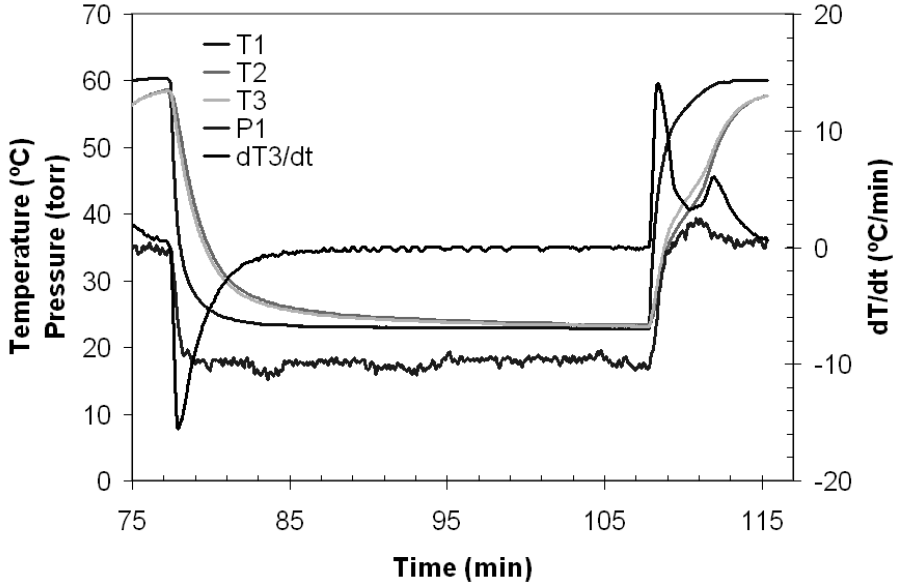

(b)

Figure 19. Pressure and temperatures profiles for adsorption/desorption cycle of the three-layer microchannel adsorption device, (a) three consecutive adsorption/desorption cycles and (b) detail of the third adsorption/desorption cycle.

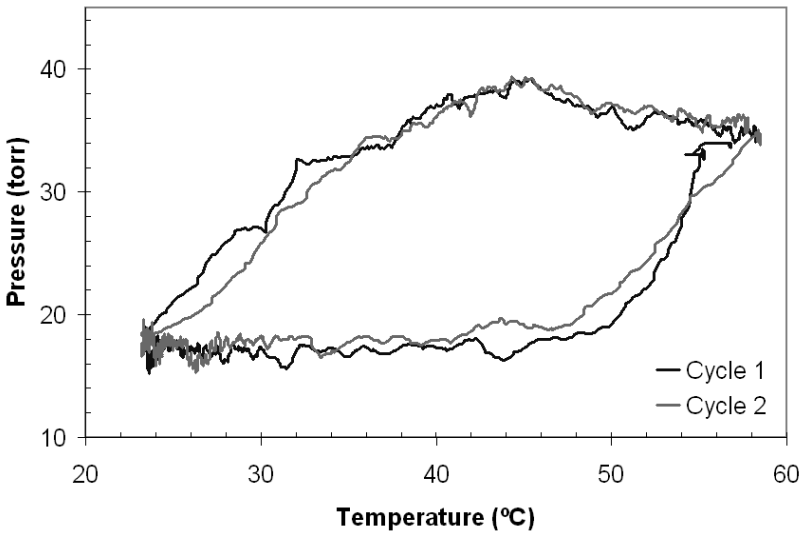

Figure 20. Pressure-temperature diagram of two successive adsorption/desorption cycles in the three-layer microchannel adsorption device.

Table 9. Base Case process input and output parameters for the three-layer microchannel adsorption cooling device.

Process parameter	Value and unit
Process input – base case	
Evaporator	
Temperature, T_{evap}	22 ºC
Pressure	19.8 torr
Condenser	
Temperature, T_{cond}	30 ºC
Pressure	31.8 torr
Dimensions of air flow channel	
Height	400 µm
Width	8.5 mm
Hydraulic diameter, D_h	760 µm
Length	4.4 cm
Air channel inlet temperature	
Adsorption stage	23 ºC
Desorption stage	60 ºC
Air channel flowrate	32.15 SLPM, 39.83 g/min
Air channel inlet pressure	1900 torr (guage)
Velocity of air in each channel	9.4 m/s at 25°C and atmospheric pressure
Calculated convective heat transfer coefficient, h	95.9 W/m^2-K
Cycle time	
Adsorption stage, t_{ads}	30 min
Desorption stage, t_{des}	7.5 min
Process output –base case	
Water sorption	
Adsorption stage (final)	0.560 ± 0.009 g water/ g silica gel
Desorption stage (final)	0.027 ± 0.005 g water/ g silica gel
Cooling output, Q_{evap}	1328 ± 20 J
Heat input for desorption, Q_{des}	2919 ± 123 J
Coefficient of performance, COP	0.455 ± 0.020
Specific cooling power, SCP	597 ± 9 W/kg silica gel

3.5 Effect of Air Flow Rate on Device Performance

The temperature profiles and cumulative heat transferred to the device during desorption stage at low and high air flow in the air flow channel during the desorption

stage are shown in Figure 21. At a lower air flow rate of 18 SLPM (5.3 m/sec at 25°C and atmospheric pressure), the required desorption time to reach steady state (t_{des}) was 12 min. In contrast, only 7.5 min were required at the higher air flow rate of 32 SLPM (9.4 m/sec at 25°C and atmospheric pressure). The average amounts of heat required to reach steady for both air flow rates were not significantly different (Table 10). The slight difference in Q_{des} between both air flow rates may be caused from heat lost from the device to the surroundings.

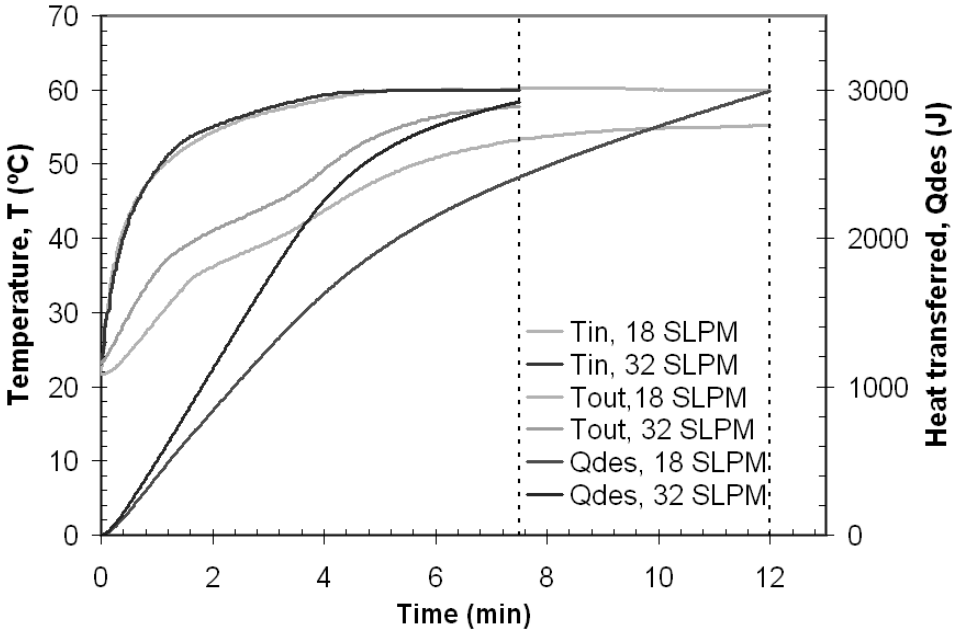

Figure 21. Temperature and cumulative heat transferred to the device versus time during a representative desorption stage at low and high air flow rates.

Process input and output parameters for the low and high air flow rates during the desorption stage are shown in Table 10. The COP calculated for both air flow rates are not significantly different, while SCP for a low-flow case is lower because of the longer desorption time. The pressure drop along the air flow channels was 850 torr for low-flow case and 1900 torr for the high-flow case.

Table 10. Comparison of process input and output parameters for low and high air flow rates during the desorption stage for the three-layer device.

Process parameter	Value and Unit	
	Low-flow case	High-flow case
Process input		
Air flow rate	17.95 SLPM	32.15 SLPM
Air velocity	5.3 m/s at 25°C and atmospheric pressure	9.4 m/s at 25°C and atmospheric pressure
Air channel inlet pressure	850 torr (guage)	1900 torr (guage)
Process output		
Amount of water adsorbed/desorbed	0.533 ± 0.009 g	0.533 ± 0.009 g
Cumulative heat transferred, Q_{des}	2992 ± 220 J	2919 ± 123 J
Coefficient of performance, COP	0.437 ± 0.033	0.448 ± 0.020
Specific cooling power, SCP	525 ± 90 W/kg silica gel	589 ± 10 W/kg silica gel
Desorption time, t_{des}	12 min	7.5 min

3.6 Effect of Hot Air Inlet Temperature on Device Performance

Figure 22 shows the amount of water transferred from the evaporator to the microchannel device in each adsorption/desorption cycle, the total amount of heat supplied during desorption stage and the performance of the device when the hot air inlet temperature to the desorption channels was changed from 50°C to 70°C. At lower hot air inlet temperature, the amount of water transferred in each cycle decreased. This was because a larger amount of water was left inside the device at the end of desorption stage. However, the heat required for desorption was significantly lower at the hot air inlet temperature of 50°C. The required heat for desorption seemed to have more impact on the COP while the amount of water transferred directly affected the SCP. From Figure 22c, the COP significantly increased when the hot air inlet temperature was lowered, while the SCP (Figure 22d) slightly increased as the hot air inlet temperature increased.

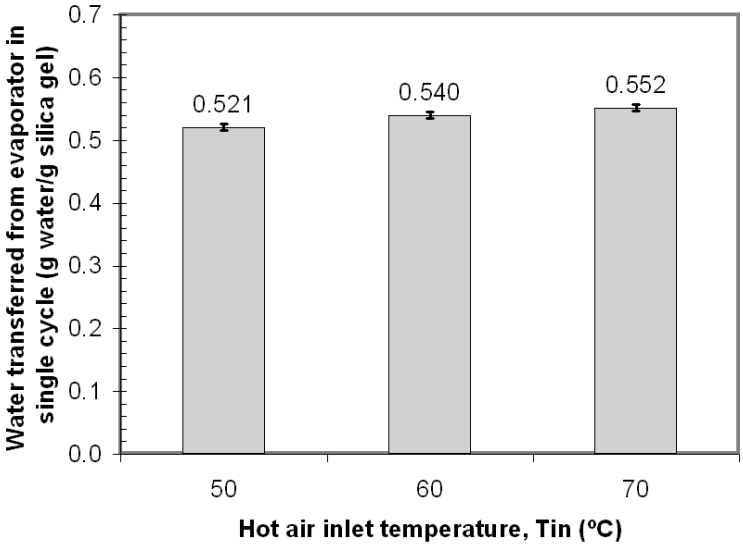

(a)

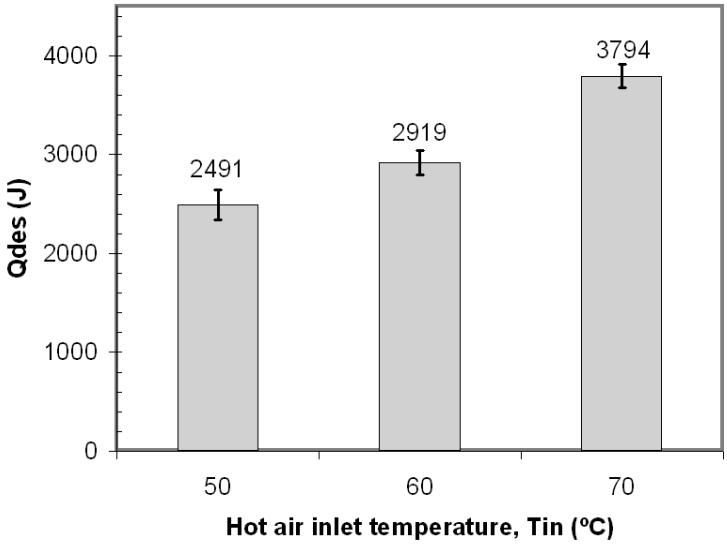

(b)

Figure 22. Effect of hot air inlet temperature on performance of the three-layer device. (a) Water transferred in each cycle, (b) heat transferred for desorption stage, (c) COP and (d) SCP.

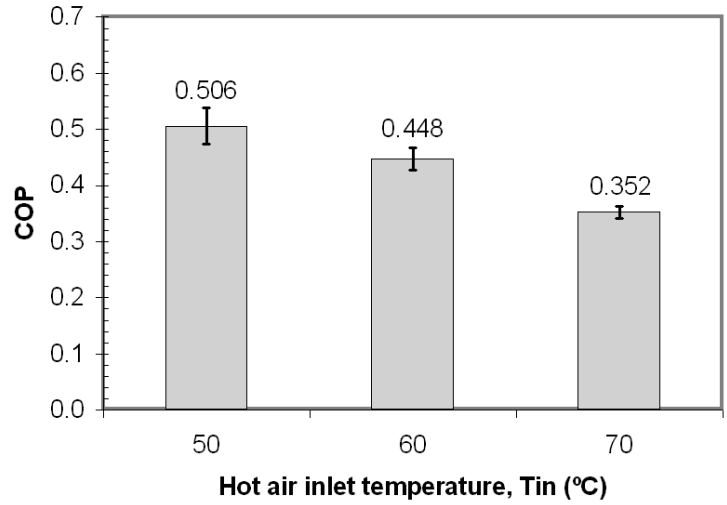

(c)

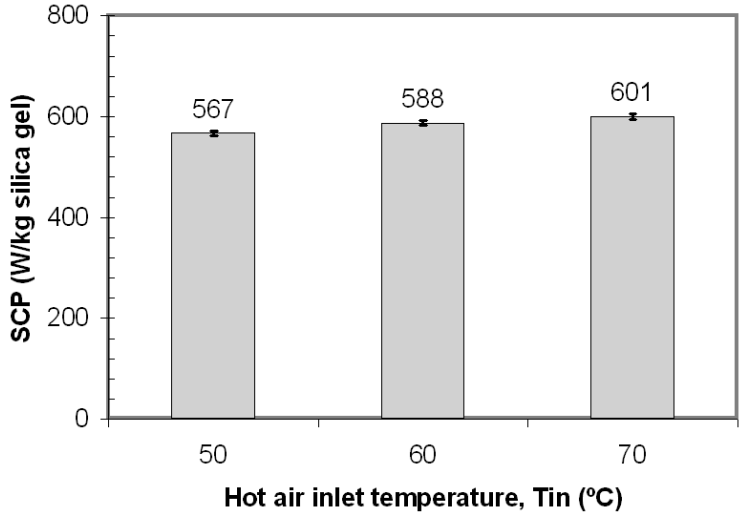

(d)

Figure 22. Effect of hot air inlet temperature on performance of the three-layer device. (a) Water transferred in each cycle, (b) heat transferred for desorption stage, (c) COP and (d) SCP. (Continued)

3.7 Effect of Microchannel Device Structure on Device Performance

Process input and output parameters for single-layer and three-layer microchannel adsorption devices are shown in Table 11. Only the input parameters that were different from Base Case of the three-layer microchannel device are presented. The device performance parameters, COP and SCP, drastically increased

when the number of adsorption layer increased. Particular, the COP increased 2.4 times and the SCP increased 1.5 times over the single-layer microchannel device.

Table 11. Comparison of process input and output parameters for single-layer and three-layer microchannel adsorption device.

Process parameter	Value and Unit	
	single-layer case	three-layer case
Process input		
Number of the adsorption layers	1 layer	3 layers
Hot air inlet temperature	70 º C	70 º C
Air flow rate	6.98 SLPM	32.15 SLPM
Air velocity	2.7 m/s at 25°C and atmospheric pressure	9.4 m/s at 25°C and atmospheric pressure
Air channel inlet pressure	500 torr	1900 torr
Desorption time, t_{des}	15 min	7.5 min
Process output		
Water transferred in single cycle	0.428 ± 0.113 g water/ g silica gel	0.552 ± 0.005 g water/ g silica gel
Amount of water adsorbed/desorbed	0.141 ± 0.038 g	0.545 ± 0.005 g
Cooling output	346 ± 92 J	1336 ± 13 J
Cumulative heat transferred, Q_{des}	2340 ± 97 J	3794 ± 118 J
Coefficient of performance, COP	0.148 ± 0.039	0.352 ± 0.011
Specific cooling power	389 ± 103 W/kg silica gel	601 ± 6 W/kg silica gel

3.8 Modeling

The modeling contains set of differential equations which are derived from mass and energy balances. These equations are then solved by Matlab. All assumptions are listed below:

- All specific heat capacities are constant;
- Latent heat of water evaporation is constant;
- Viscosity of air is constant;
- Water vapor is ideal gas;
- Water adsorbed into silica gel behaves like water liquid;

- Air inlet temperatures during adsorption/desorption are constant;
- Initial water uptake at the end of desorption stage is at equilibrium;
- The velocity profile in air flow channels is fully developed; and
- Temperature inside the microchannel device is uniform.

The mass balance on the device is done on both phases of water which are water vapor and water adsorbed on silica gel. Mass balances on the other species, such as the aluminum housing, adsorbent material and flowing air, are not necessary because those species do not accumulate in the system. The mass balance of water vapor is shown in equation (10), given by

$$\dot{m}_{wv,ev} - \dot{m}_{wv,cd} - r_{adsorption} m_{sg} = \frac{d\, m_{wv,adsorber}}{dt} \tag{10}$$

where $\dot{m}_{wv,ev}$ is the mass flow rate of water vapor from an evaporator (g/min), $\dot{m}_{wv,cd}$ is the mass flow rate of water vapor to a condenser (g/min), $r_{adsorption}$ is the adsorption rate (g silica gel/g water-min), m_{sg} is the amount of silica gel (g) and $m_{wv,adsorber}$ is the amount of water in the vapor phase (g). Since water vapor is assumed to be an ideal gas, the ideal gas law is applied to equation (10), so that

$$\dot{m}_{wv,ev} - \dot{m}_{wv,cd} - r_{adsorption} m_{sgt} = \left(\frac{V}{MW_w R} \right) \frac{d}{dt} \left(\frac{P}{T} \right) \tag{11}$$

where V is vapor phase volume of the device (m^3), MW_W is molecular weight of water (g/mol), R is the ideal gas constant (J/mol-K), P is pressure inside the adsorption channels (torr)and T is temperature of the device (K). The mass balance of water that is adsorbed onto the adsorbent layer is given by

$$r_{adsorption} = \frac{dL}{dt} \tag{12}$$

where L is the water uptake or amount of water adsorbed per unit mass of adsorbent.

The energy balance of the adsorption device is give by

$$\dot{q} - \dot{q}_{lost} + U_{wv,ev}\dot{m}_{wv,ev} - U_{wv,adsorber}\dot{m}_{wv,cd} = \frac{d}{dt}\left(m_{al}U_{al}\right) + \frac{d}{dt}\left(m_{sg}U_{sg}\right) + \frac{d}{dt}\left(m_{wv,adsorber}U_{wv,adsorber}\right) + \frac{d}{dt}\left(m_{wa}U_{wa}\right) \quad (13)$$

where $\dot{q}$ is rate of heat transfer from air flow channels to adsorption channels (J/min), $\dot{q}_{lost}$ is rate of heat lost from the device to atmosphere (J/min), $U_{wv,ev}$ is internal energy of water vapor flowing from evaporator to the adsorption channels (J/g), $U_{wv,adsorber}$ is internal energy of water vapor desorbed out of adsorbent material and flowing to condenser (J/g), $m_{al}U_{al}$ is total internal energy of the aluminum housing (J), $m_{sg}U_{sg}$ is total internal energy of the dry adsorbent material (J), $m_{wv,adsorber}U_{wv,adsorber}$ is total internal energy of the dry adsorbent material (J), and $m_{wa}U_{wa}$ is total internal energy of the dry adsorbent material (J).

After application of the ideal gas law and rearrangement of equation (13), the final version of the energy balance is

$$\dot{q} - \dot{q}_{lost} + \left(T_{ev} - T\right)C_{v,wv}\dot{m}_{wv,ev} - r_{adsorption}m_{sg}\Delta U_{adsorption} = \left(m_{al}C_{p,al} + m_{sg}C_{p,sg} + \frac{PV}{MW_w RT}C_{v,wv} + Lm_{sg}C_{p,wa}\right)\frac{dT}{dt} \quad (14)$$

where T_{ev} is evaporator temperature (K), $C_{v,wv}$ is specific heat capacity of water vapor (J/g-K), $\Delta U_{adsorption}$ is change in internal energy of water adsorption (J/g), m_{al} is mass of aluminum housing (g), $C_{p,al}$ is specific heat capacity of aluminum (J/g-K), $C_{p,sg}$ is specific heat capacity of dry silica gel (J/g-K), and $C_{p,wa}$ is specific heat capacity of

water adsorbed on silica gel (J/g-K). The complete derivation of energy balance can be found in Appendix D.

Besides the mass and energy balance equations above, there are several constitutive equations to be considered. The rate of heat supplied to/removed from the system, $\dot{q}$, can be calculated using equation (15) and (16)

$$\dot{q} = \dot{m}_{air} C_{p,air} \left(T_1 - T_2\right) \tag{15}$$

where $\dot{m}_{air}$ is mass flow rate of air (g/min), $C_{p,air}$ is specific heat capacity of air (J/g), and T_1 and T_2 are temperatures of air flow inlet and outlet (K), respectively.

$$\dot{q} = UA_q \Delta T_{lm} \tag{16}$$

where U is an overall heat transfer coefficient (W/m^2-K), A_q is an area of heat transfer in air flow channels (m^2) and ΔT_{lm} is a log-mean temperature difference between air flow channels and adsorption channels (T), given by

$$\Delta T_{lm} = \frac{T_1 - T_2}{\ln\left(\dfrac{T_1 - T_3}{T_2 - T_3}\right)} \tag{17}$$

where T_1, T_2 and T_3 are temperatures of air flow inlet, air flow outlet and the device, respectively (K). T_2 can be obtained by combining equation (15) and (16).

$$T_2 = \left(T_1 - T_3\right) e^{\frac{-UA}{\dot{m}_{air} C_{p,air}}} + T_3 \tag{18}$$

The overall heat transfer coefficient (U) is defined by

$$\frac{1}{U} = \sum_i \frac{l_i}{k_i} + \frac{1}{h_{air}} \tag{19}$$

where l_i is a thickness of each layer between air flow channel and adsorbent layer (m), k_i is a thermal conductivity of each layer between air flow channel and adsorbent layer (W/m-K), and h_{air} is a convective heat transfer coefficient for the air flow channels (W/m^2-K). The convective heat transfer coefficient (h_{air}) can be calculated from

$$h_{air} = \frac{k_{air}\,\mathrm{Nu}}{D_h} \tag{20}$$

where k_{air} is thermal conductivity of air, Nu is Nusselt number, and D_h is hydraulic diameter of each rectangular air flow channel, which is given by

$$D_h = \frac{2(w \cdot h)}{(w + h)} \tag{21}$$

where w is width of each channel and h is height of each channel. The Nusselt number for developing laminar flow in a tube and constant wall temperature can be calculated by Seider-Tate correlation

$$\mathrm{Nu} = 1.86\left(\frac{D_h\,\mathrm{Re}\,\mathrm{Pr}}{L}\right)^{1/3} \tag{22}$$

where Re is the Reynolds number, and L is a length of each channel. Pr is the Prandtl number, defined by

$$\mathrm{Pr} = \frac{C_{p,air} \cdot \mu_{air}}{k} \tag{23}$$

where $C_{p,air}$ is a specific heat of air, μ_{air} is a viscosity of air, and k_{air} is a thermal conductivity of air. The Reynolds number (Re) is defined by

$$\mathrm{Re} = \frac{D_h \dot{m}_{air}}{\mu_{air} A_{cross} n_{air\ channel}} \tag{24}$$

where A_{cross} is the cross-sectional area of each air flow channel, and n_{air} channel is the number of air flow channels in the device. The rate of heat lost can be calculated by

$$\dot{q}_{lost} = U_{lost} A_{lost} \left(T - T_{room} \right) \tag{25}$$

where U_{lost} is an overall heat transfer coefficient for heat lost, A_{lost} is an area of the device outer surface that exposed to room temperature and T_{room} is a room temperature. Because the heat lost is limited by the conductivity of thick insulator, U_{lost} can is defined by

$$U_{lost} = \frac{k_{insulator}}{l_{insulator}} \tag{26}$$

where $k_{insulator}$ is thermal conductivity of insulator, and $l_{insulator}$ is thickness of insulator layer. Adsorption rate ($r_{adsorption}$) can be calculated by

$$r_{adsorption} = k\left(L^{*} - L \right) \tag{27}$$

where k is an adsorption rate constant L is an instantaneous water uptake, and L^{*} is the equilibrium water uptake, given by

$$L^{*} = A\left(\frac{P}{Psat} \right)^{B} \tag{4}$$

Equation (28) is the Antoine equation which describes the relation of the saturated vapor pressure (P_{sat}) and the temperature (T) and is given by

$$P_{sat} = 10^{A - \frac{B}{T+C}} \tag{28}$$

where A, B and C are component specific constants for water.

Balance equations (11), (12) and (14) must be modified to suit specific conditions of each adsorption/desorption step.

In Step 1 (isolated adsorption) the adsorption channels are isolated. There is no water flow from the evaporator nor to the condenser, $\dot{m}_{wv,ev} = 0$ and $\dot{m}_{wv,cd} = 0$. An energy balance equation (14) and a water adsorbed balance equation (12) can be rewritten as

$$\frac{dT}{dt} = \frac{\dot{q} - \dot{q}_{lost} - r_{adsorption} m_{sg} \Delta U_{adsorption}}{m_{al} C_{p,al} + m_{sg} C_{p,sg} + \frac{PV}{MW_w RT} C_{v,wv} + L m_{sg} C_{p,wa}} \tag{29}$$

$$\frac{dL}{dt} = r_{adsorption} \tag{30}$$

The water vapor balance (equation (11)) becomes

$$\frac{dP}{dt} = -r_{adsorption} m_{sg} \left(\frac{MW_W RT}{V} \right) + \left(\frac{P}{T} \right) \frac{dT}{dt} \tag{31}$$

Substitution of equation (29) into equation (31) yields

$$\frac{dP}{dt} = -r_{adsorption} m_{sg} \left(\frac{MW_W RT}{V} \right) + \left(\frac{P}{T} \right) \frac{\dot{q} - \dot{q}_{lost} - r_{adsorption} m_{sg} \Delta U_{adsorption}}{m_{al} C_{p,al} + m_{sg} C_{p,sg} + \frac{PV}{MW_w RT} C_{v,wv} + L m_{sg} C_{p,wa}} \tag{32}$$

Equations (29), (30) and (32) are solved to obtain temperature (T), pressure (P) and water uptake (L) at anytime during isolated adsorption step.

Step 2 (active adsorption) starts when pressures in the adsorber channels and evaporator are equal. During Step 2, pressure in the adsorption channel is kept constant, $\frac{dP}{dt} = 0$, and is controlled by the temperature in an evaporator. The valve to

the evaporator is opened so that $\dot{m}_{wv,ev} \neq 0$, while the valve to a condenser is still closed so that $\dot{m}_{wv,cd} = 0$. Equations (12), (11) and (14), respectively, become

$$\frac{dL}{dt} = r_{adsorption} \tag{30}$$

$$\frac{dT}{dt} = \frac{MW_w RT^2}{PV}\left(r_{adsorption} m_{sg} - \dot{m}_{wv,ev}\right) \tag{33}$$

$$\frac{dT}{dt} = \frac{\dot{q} - \dot{q}_{lost} + (T_{ev} - T)C_{v,wv}\dot{m}_{wv,ev} - r_{adsorption} m_{sg} \Delta U_{adsorption}}{m_{al}C_{p,al} + m_{sg}C_{p,sg} + \frac{PV}{MW_w RT} C_{v,wv} + Lm_{sg}C_{p,wa}} \tag{34}$$

Equations (33) and (34) contain two unknown variables, $\frac{dT}{dt}$ and $\dot{m}_{wv,ev}$. Both equations are combined and $\dot{m}_{wv,ev}$ is eliminated. The combined equation is given by

$$\frac{dT}{dt} = \frac{r_{adsorption} m_{sg} + \frac{\dot{q} + \dot{q}_{lost} + r_{adsorption} m_{sg} \Delta U_{adsorption}}{(T_{ev} - T)C_{v,wv}}}{\frac{1}{(T_{ev} - T)C_{v,wv}}\left(m_{al}C_{p,al} + m_{sg}C_{p,sg} + \frac{PV}{MW_w RT} C_{v,wv} + Lm_{sg}C_{p,wa}\right) - \frac{PV}{MW_w RT^2}} \tag{35}$$

There are only 2 differential equations, (30) and (35), that need to be solved for temperature and water uptake, in the active adsorption step. The pressure is constant and Step 2 ends when the desorption time (t_{des}) has reached.

Step 3 (isolated desorption) requires same set of equations as Step 1. Equations (29), (30) and (32) are also solved to obtain temperature (T), pressure (P) and water uptake (L) at anytime during isolated desorption step.

Step 4 (active desorption) starts when pressures in the adsorption channels and the condenser are equal. In contrast of the continued adsorption step, the valve to a condenser is opened, so that $\dot{m}_{wv,cd} \neq 0$, while the valve to an evaporator is kept

closed, so that $\dot{m}_{wv,ev} = 0$. Because pressure is constant, only two equations below are required and given by

$$\frac{dL}{dt} = r_{adsorption} \tag{30}$$

$$\frac{dT}{dt} = \frac{\dot{q} - \dot{q}_{lost} - r_{adsorption} m_{sg} \Delta U_{adsorption}}{\left(m_{al} C_{p,al} + m_{sg} C_{p,sg} + \frac{PV}{MW_w RT} C_{v,wv} + L m_{sg} C_{p,wa} \right)} \tag{36}$$

The set of differential equations for each step was written in Matlab. The source code is provided in Appendix E. Input parameters, constant parameters and output parameters are listed in Table 12, 13 and 14, respectively.

Table 12. Input parameters for Matlab simulation of process model.

Parameter	Description	Symbol in Matlab	Base Case value	Unit
$\dot{m}_{air}$	Mass flow rate of air	mair	38.94	g/min
$T_{a,in,cool}$	Air inlet temperature during the adsorption stage	Taincool	23	°C
$T_{a,in,hot}$	Air inlet temperature during the desorption stage	Tainhot	70	°C
T_{cd}	Temperature inside a condenser	Tcd	30	°C
T_{ev}	Temperature inside an evaporator	Tev	22	°C
T_{room}	Room temperature	Troom	23	°C
t_{ads}	Adsorption time per cycle	tads	30	min
t_{des}	Desorption time per cycle	tdes	7.5	min

Table 13. Constant parameters for Matlab simulation of process model.

Parameter	Description	Symbol in Matlab	Value	Unit
ΔH_{evap}	Enthalpy of water evaporation	dHevap	2442.5	J/g
ΔH_{ads}	Internal energy of water adsorption	dUadsorption	-2800	J/g
μ_{air}	Viscosity of air	muair	18.27×10^{-3}	g/m-s
$C_{P,air}$	Specific heat capacity of air	Cpair	1.012	g-K
$C_{P,al}$	Specific heat capacity of aluminum	Cpal	0.897	J/g-K
$C_{P,sg}$	Specific heat capacity of silica gel	Cpsg	0.740	J/g-K
$C_{P,wa}$	Specific heat capacity of water adsorbed on silica gel	Cpwa	4.185	J/g-K
$C_{v,wv}$	Specific heat capacity of water vapor	Cvwv	1.4	J/g-K
h	Height of each air flow channel	hD	0.016	in
k_{air}	Thermal conductivity of air	kair	0.02	W/m-K
l	Length of each air flow channel	lD	1.73	in
m_{al}	Mass of aluminum housing	mal	39.694	g
m_{sg}	Mass of dry silica gel	msg	0.9882	g
MW_w	Molecular weight of water	MWw	18.015	g/mol
R	Ideal gas constant	R1 R2	8.314 62363.67	J/mol-K cm^3-torr /mol-K
V	Volume of vapor phase in the device	V	6.71	cm^3
w	Width of each air flow channel	wD	0.23	in

Table 14. Output parameters from process model calculations.

Parameter	Description	Symbol in Matlab	Unit
$L(t)$	Water uptake	L	g water/g silica gel
$P(t)$	Pressure	P	torr
$T(t)$	Temperature	T	°C
COP	Coefficient of performance	COP	-
SCP	Specific cooling power	SCP	W/kg silica gel

The simulation result of Base Case operation is shown in Figure 23 and 24. Figure 23a shows the pressure and temperatures profiles. The temperature and pressure profiles in Figure 23a follow the same trend as the experimental result. Step 1 (isolated adsorption) takes 21 sec while Step 3 (isolated desorption) lasts only 14 sec. The instantaneous water uptake, which was not obtain by experiment, is presented in Figure 23b. The equilibrium uptake is also estimated from adsorption isotherm so the adsorption driving force, L_{eq}-L, can be determined.

Figure 23c presents how the accumulated heat during adsorption and desorption stages is calculated. During the adsorption stage (0-30 min), heat needs to be removed and, so the calculated heat transferred becomes negative. For the desorption stage (after 30 min), the external heat by hot air flow is provided so that the calculated heat transferred is positive. The heat transferred at 37.5 min is 2600 J, which is the total heat required for the desorption stage (Q_{des}).

From the simulation result, the device seems to have a problem in cooling down to room temperature. It takes less than 3 min to reach 30°C from the initial temperature of 60°C, but takes additional 5 min to lower the device temperature from 30°C to 25°C. Therefore, the modeling results suggest that the cooling method during the adsorption stage should be improved.

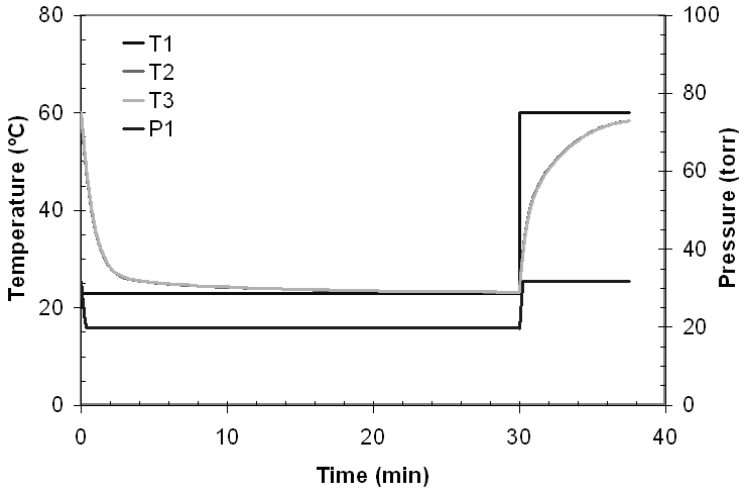

(a)

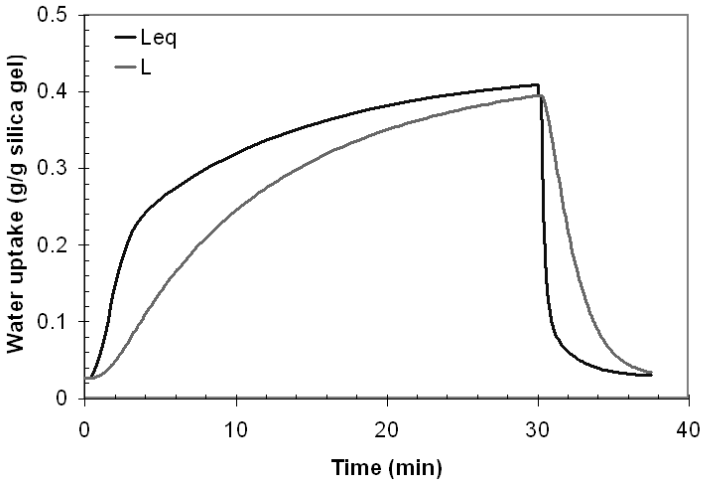

(b)

Figure 23. Predicted pressure, temperature, water uptake and heat transferred vs. time profiles at the Base-case operating conditions. (a) Pressure and temperature, (b) water uptake and equilibrium water uptake and (c) temperature and heat transferred.

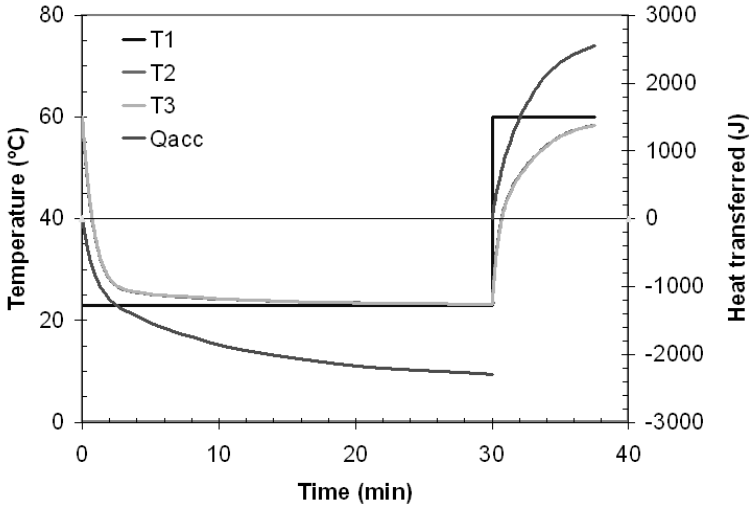

(c)

Figure 23. Predicted pressure, temperature, water uptake and heat transferred vs. time profiles at the Base-case operating conditions. (a) Pressure and temperature, (b) water uptake and equilibrium water uptake and (c) temperature and heat transferred. (Continued)

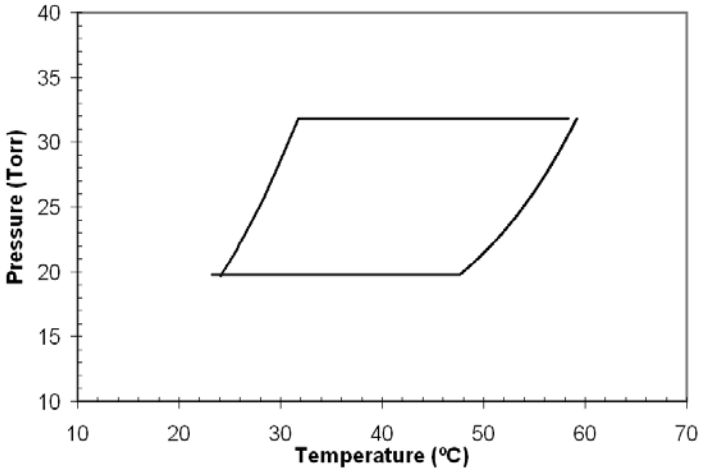

Figure 24. Predicted pressure and temperature diagram at the Base-case operating conditions.

The predicted COP and SCP are sensitive to many variables. In the simulation study, three parameters were varied: 1) hot air inlet temperature, 2) evaporator temperature, and 3) mass ratio of aluminum housing to silica gel adsorbent.

The predicted COP and SCP vs. hot air inlet temperatures to the desorption air channel are shown in Figure 25. The COP is maximized at hot air inlet temperature about 40°C. The COP decreases more rapidly at temperature below 40°C. The SCP does not change much with temperature between 70°C and 90°C. The SCP becomes very low at temperatures close to 30°C, the condenser temperature.

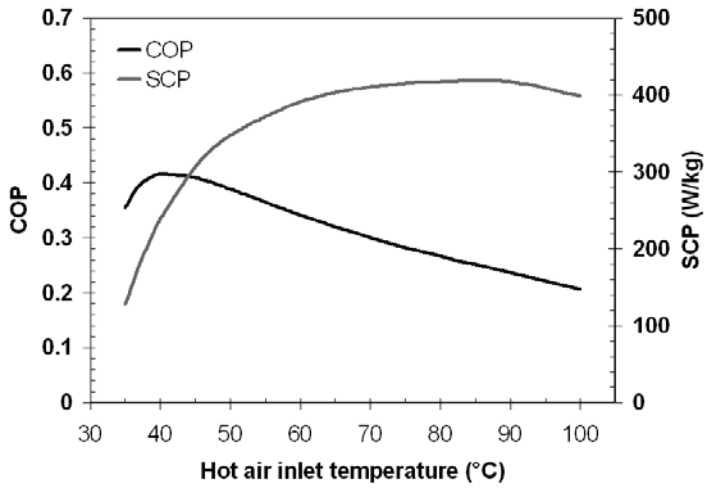

Figure 25. Predicted COP and SCP of the adsorption cooling device vs. hot air inlet temperature.

The predicted COP and SCP vs. evaporator temperature are shown in Figure 26. The trends of COP and SCP are quite similar. The performance of the device is better when evaporator temperature is at 22°C (or closet to adsorption temperature of 23°C). At the evaporator temperature of 12°C or below, the vapor pressure of water is not significant enough to adsorb any appreciable amount of water on the silica gel, and so the COP and SCP are close to zero.

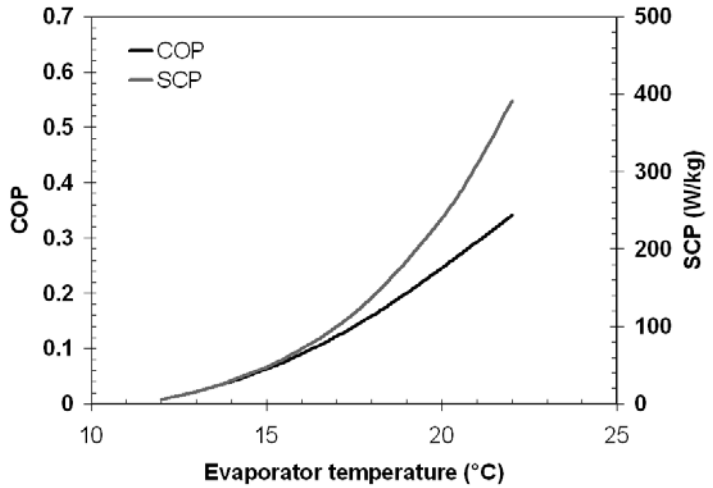

Figure 26. Predicted COP and SCP of the adsorption cooling device vs. evaporator temperature.

The effect of aluminum to silica gel mass ratio on COP and SCP are compared in Figure 27. The SCP is insensitive to the mass ratio, but the COP improves when the aluminum to silica gel ratio decreases.

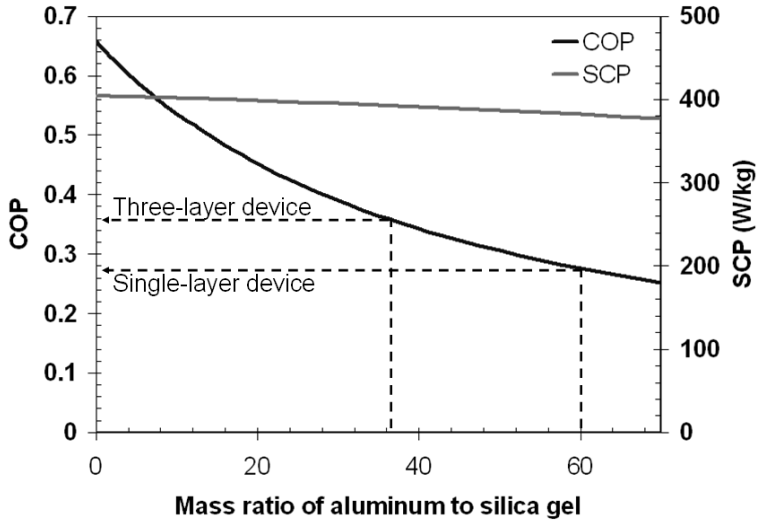

Figure 27. Predicted COP and SCP of the adsorption cooling device vs. mass ratio of aluminum to silica gel.

Chapter 4 - Summary and Conclusions

4.1 Effect of Air Flow Rate on Device Performance

Increasing the hot air flow rate to the air flow channels during the desorption stage improves the overall performance of the device. Increasing the hot air flow rate causes the device reach the set point temperature faster, so that the cycle time can be decreased. One important point to mention is that the COP is not cycle time dependent, while the SCP is. When desorption time (t_{des}) decreases, the SCP improves but nothing happens to the COP. Increasing the air flow rate has no effect on the amount of water adsorbed/desorbed in each cycle. However, the COP gets improved slightly because the total heat lost in single cycle decreases. In this work, COP increased from 0.437 to 0.448 while SCP increased from 525 to 589 W/kg silica gel when the air flow rate was increased by a factor of 1.8 (Table 10). The heat lost was minimized by insulating the outer surface of the device. In this work, Kaowool ceramic insulator was used. If the device is sufficiently insulated, COP should not change significantly with air flow rate, which was observed experimentally.

4.2 Effect of Hot Air Inlet Temperature on Device Performance

From the experimental result given in Figure 22, decreasing the hot air inlet temperature from 70°C to 50°C during the desorption stage increases the COP but decreases the SCP. Lowering the hot air temperature causes the amount of water that is left on the silica gel layer after the end desorption stage to decrease, according to the water adsorption equilibrium. This also means that the amount of water evaporated in single cycle is getting lower. Therefore, lower SCP is expected, because the SCP is directly proportional to the amount of water transferred in each cycle. In contrast, the trend of COP is different from that of SCP because the value of COP is affected by two factors: 1) the amount of water transferred in each adsorption/desorption cycle (m_{evap}), and 2) the total heat supplied to the device during desorption stage (Q_{des}). Decreasing the desorption temperature will decrease both m_{evap} and Q_{des}, and

therefore affects COP. Specifically, COP is an increasing function of m_{evap} but is a decreasing function of Q_{des}. Based on the experimental results from this work, decreasing the hot air inlet temperature causes an increase of COP. This means that the Q_{des} term has more contribution to COP than m_{evap} does. This COP trend agrees with Boelman's work [6] but not with all other previous work. The explanation for this conflict is that heat transferred to the device during desorption, Q_{des}, is consumed by three components, the heat of water desorption, the sensible heat change of the device with temperature, and the heat lost to surroundings. In most of the previous studies, the heat of water desorption is more dominant than the other two components because the mass ratio of metal to adsorbent for conventional adsorption cooling system is about 4 or less with inferior heat transfer, while the ratio for this study is 40 with superior heat transfer. For this reason, the sensible heat component of Q_{des} in this study is more dominant compared to the previous work. If the metal to adsorbent ratio is minimized, then the sensible heat change will become less important.

4.3 Effect of Number of Adsorption Layers on Device Performance

The principal difference between the single-layer and three layer devices is the mass ratio of metal housing to adsorbent material. The ratio is 65 for single-layer device and 40 for three-layer device. The decrease in the metal to adsorbent ratio leads to increase in COP, as mentioned in section 4.2. Based on the current design, the ratio approaches 31 when a large number of adsorption layers (13) was reached. Although the air flow rates of the single-layer and three-layer devices (Table10), the results between single-layer and three-layer devices were still comparable because the air flow rate did not significantly affect the COP, as mentioned in section 4.1.

4.4 Direct Performance Comparison of this Work to Previous Work

It is very difficult to compare performance between adsorption cooling devices due to the different design of each device itself and its operating parameters, such as ratio of metal housing to adsorbents material, type of adsorbent used, evaporator temperature, cooling fluid temperature, heating fluid temperature and cycle time. According to the literature review in Table 2, COPs range from 0.1 to 0.5 depending on the operating temperatures while SCPs are generally under 100 W/kg. In the Base Case operation of the three-layer microchannel adsorption device, a COP of 0.488 and a SCP 589 W/kg are obtained. The SCP of this work is considerably higher compared to previous work because the evaporation temperature in this work is high. From the simulation results, SCP decreases significantly when the evaporation temperature is decreased.

In summary, the SCP improves when microchannel technology is applied. However, the COP is still comparable to most of recent studies because the mass ratio of metal housing to adsorbent material is high. However, this is the first generation of microchannel adsorption devices for adsorption cooling applications and future studies might consider more layers to reduce the metal to adsorbent ratio.

Bibliography

[1] Plank R, Kuprianoff J, In Die Kleinkältemaschine. Springer-Verlag, Berlin/Göttingen/Heidelberg, 1960

[2] Kester FL, Lunde PJ, Chemisorption-B.E.T. Model for adsorption of water vapor on silica gel, AIChE symposium series, 69(134), 87-94

[3] Anyanwu EE, Review of solid adsorption solar refrigeration II: An overview of the principles and theory, Energy Conversion and Management, 2004, 45, 1279-1295

[4] Critoph RE, Activated carbon adsorption cycles for refrigeration and heat pumping, Carbon, 1989, 27(1), 63-70

[5] Srivastava NC, Eames IW, A review of developments in solid-vapour adsorption-refrigeration and heat-pump systems, Journal of the Institute of Energy, 1997, 70(485), 116-127

[6] Boelman EC, Saha BB, Kashiwagi T, Experimental investigation of a silica gel-water adsorption refrigeration cycle – The influence of operating condition on cooling output and COP, ASHRAE Transactions, 1995, 101(2), 358-366

[7] Akahira A, Alam KCA, Hamamoto Y, Akisawa A, Kashiwagi T, Mass recovery adsorption refrigeration cycle—improving cooling capacity, International Journal of Refrigeration, 2004, 27(3), 225-234

[8] Wang X, Chua HT, Ng KC, Experimental investigation of silica gel–water adsorption chillers with and without a passive heat recovery scheme, International Journal of Refrigeration, 2005, 28(5), 756-765

[9] Kong XQ, Wang RZ, Wu JY, Huang XH, Huangfu Y, Wu DW, Xu YX, Experimental investigation of a micro-combined cooling, heating and power system driven by a gas engine, International Journal of Refrigeration, 2005, 28(7), 977-987

[10] Wang, DC, Shi ZX, Yang QR, Tian, XL, Zhang, JC,Wu JY, Experimental research on novel adsorption chiller driven by low grade heat source, Energy Conversion and Management, 2007, 48(8), 2375-2381

[11] Xia Z, Wang D, Zhang J, Experimental study on improved two-bed silica gel-water adsorption chiller, Energy Conversion and Management, 2008, 49(6), 1469-1479

[12] Yang GZ, Xia ZZ, Wang RZ, Keletigui D, Wang DC, Dong ZH, Dong ZH, Yang X, Research on a compact adsorption room air conditioner, Energy Conversion and Management, 2006, 47(15-16), 2167-2177

[13] Ng KC, Sai MA, Chakraborty A, Saha BB, Koyama S, The electro-adsorption chiller: Performance rating of a novel miniaturized cooling cycle for electronics cooling, Journal of Heat Transfer, 2006, 128(9), 889-896

[14] Daou K, Wang RZ, Xia ZZ, Yang GZ, Experimental comparison of the sorption and refrigerating performances of a CaCl2 impregnated composite adsorbent and those of the host silica gel, International Journal of Refrigeration, 2007, 30(1), 68-75

[15] Cui Q, Chen H, Tao G, Yao H, Performance study of new adsorbent for solid desiccant cooling, Energy, 2005, 30(2-4), 273-279

[16] Wang SG, Wang, RZ, Li XR, Research and development of consolidated adsorbent for adsorption systems, Renewable Energy, 2005, 30(9), 1425-1441

[17] Yong L, Wang RZ, Adsorption refrigeration : A survey of novel technologies, Recent Patents on Engineering, 2007, 1(1), 1-21

[18] Ehrfeld W, Hessel V, Löwe H, Microreactors : New Technology for Modern Chemistry, Wiley-VCH, 2000

[19] Harpole GM, Eninger JE, Micro-channel heat exchanger optimization, Proceedings - IEEE Semiconductor Thermal and Temperature Measurement Symposium, 1991, 59-63

[20] Wang W, Jia JY, Li ZW, Fan CQ, A microchannel experimental apparatus for heat exchanging: Design and analysis, 2005 IEEE Networking, Sensing and Control, ICNSC2005 – Proceedings, 2005, 60-64

[21] Brandner JJ, Anurjewa E, Bohna L, Hansjostena E, Henninga T, Schygullaa U, Wenkaa A, Schuberta K, Concepts and realization of microstructure heat exchangers for enhanced heat transfer, Experimental Thermal and Fluid Science, 2006, 30(8), 801-809

[22] Jiang J, Hao Y, Shi Mi, Fluid flow and heat transfer characteristics in rectangular microchannels, Heat Transfer - Asian Research, 2008, 37(4), 197-207

[23] Perry RH, Green DW, Maloney JO, Perry's Chemical Engineers' Handbook, McGraw-Hill, 1997

[24] Saha BB, Akisawa A, Kashiwagi T, Silica gel water advanced adsorption refrigeration cycle, Energy, 1997, 22(4), 437-447

[25] Sakoda D, Suzuki M, Fundamental study on solar powered adsorption cooling system, Journal of Chemical Engineering of Japan, 1984, 17(1), 52-57

[26] Smith JM, Van Ness HC, Abbott MM, Introduction to Chemical Engineering Thermodynamics, McGraw Hill, 2001

[27] Janna WS, Engineering Heat Transfer, CRC Press, 2000

[28] Matheson Tri-Gas, Inc., http://www.mathesontrigas.com

APPENDICES

Appendix A - Procedures

Adsorption Isotherm

Part 1 Exposing to saturated water vapor to bare silica gel TLC plate

1. Place TLC plate in the oven at 100°C for water desorption for 10 min
2. Weigh a silica gel TLC plate
3. Place TLC plate in the water vapor-saturated environment at controlled temperature for 1 hr (In this research, TLC plate was placed inside the closed container with excess amount of liquid water.)
4. Weigh a silica gel TLC plate
5. Repeat Step 1-4 again with same or different adsorption temperatures
6. When finish all adsorption experiments, take a TLC plate into a furnace at 400°C to desorb water out as much as possible
7. Weigh a silica gel TLC plate as soon as it is taken out of the surface. This is going to be the weight of dry silica gel and aluminum support
8. Scrap all coated silica gel out of TLC plate
9. Weigh a bare aluminum support.

The water uptake can be calculated when weight of each TLC component is known.

Part 2 Flowing superheated water vapor through a microchannel adsorption device

1. Flow hot air through the adsorption channels of adsorption device for water desorption for 10 min
2. Weigh a device at fully desorbed condition
3. Flow air with specified partial pressure of water through the device at controlled temperature for 30 min (In this research, the superheated water vapor is generated by flow air pass through a water liquid at low temperature and heat the saturated air at low temperature to superheated air at higher temperature.)
4. Weigh a device at fully adsorbed condition

5. Repeat Step 1-4 again with same or different adsorption temperatures and/or partial pressure of water

The water uptake can be calculated when weights of water adsorbed and amount of silica gel in the device are known

Microchannel Adsorption Device Fabrication

Part 1 Epoxy films preparation

- Take the epoxy adhesive films on of the freezer, make sure the films are at (or close) to room temperature before taking them out of the package. The films are very brittle at low temperature
- Cut the epoxy adhesive films using a laser cutter

Part 2 Aluminum shims preparation

- Since the top and bottom plates are not laser-cut, use sheer cutter to cut the top and bottom plates and make sure that the cut plates can fit on a fixture.
- Drill 2 holes on the top plate for adsorption channel inlet and outlet.
- Remove all burrs occurred from machining.
- Place all aluminum shims into a container of 1:1 by volume acetone and methanol mixture.
- Put the container in a bath sonicator for 30 min.
- Let all shims dry before transferring adhesive films onto them.

Part 3 Stacking and bonding

- Put on hand gloves to prevent oil from skin sticking on the aluminum and adhesive film surfaces
- Heating up the aluminum shim to 70-90°C (using a hot plate)
- Locate the adhesive film onto one side of the aluminum shim. Make sure that the adhesive film, not a wax paper, facing to the aluminum shim. Align by eye and apply pressure to the adhesive film and aluminum shim using finger. Do not remove a wax paper until the shim is ready to be stacked.

- Place the same aluminum shim back on a heater and transfer the adhesive film to another side of the shim.
- Transfer the adhesive films to both sides of all other aluminum shims
- Spray boron nitride aerosol onto a fixture to prevent top and bottom plates sticking to a fixture
- Remove wax papers from shims and stack the aluminum shims on the fixture
- After stacking all shims on a fixture, place a drilled graphite brick over a fixture and clamp the fixture and a top brick with spring clamp. Do not use a screw clamp because it is getting loose after the adhesive film starting to melt and flow. Alternatively, dead weight can be put to the top of the fixture as a pressure source.
- Place the whole element inside the oven at 130°C for 2 hr

Part 4 Connectors

- Cleaning the joining spots with sand paper
- Align all connectors on the bonded device and glue them together using J-B Weld glue. After applying the glue, it is recommended to blow the hot air onto joining spots. This will help glue to adhere better and removing air out of the joining spots.
- Allow 24 hrs. for J-B Weld glue to cure before placing the device on the test loop.

Adsorption Rate

1. Desorb water out of the microchannel adsorption device by simultaneously flowing hot air through the air flow channels and pulling vacuum on the adsorption channels.
2. Isolate the adsorption channels at the end of desorption step
3. Wait until the device cooling down to the desired temperature, open the valve that connects adsorption channels and the evaporator (at the same controlled temperature) together. Start the timer

4. Wait until the set time elapsed, close the valve.
5. Take the adsorption device off and weigh as soon as possible
6. Repeat Step 1-5 with same or different temperatures

Use amount of water adsorbed in single adsorption cycle and known amount of dry silica gel in the device to calculate a water uptake at that operating temperature

Adsorption/Desorption Cycle

1. Open water circulators of the evaporator and condensers. Wait until temperatures of the evaporator and condenser are at the set points.
2. Open valves connected to the evaporator (V1) and to the condenser (V2b). Turn on the vacuum pump and open valve to the vacuum pump (V3). This will remove air out of the system.
3. Make sure that valves to the evaporator (V1) and to the condenser (V2b) are then closed. Flow hot air through the air flow channels of the device.
4. Wait until temperature reaches the steady point, turn on the vacuum pump and open the valve connected to the vacuum pump (V2a) for 5-10 min. This will remove the residual air out of the device.
5. Close all valves connected to the vacuum pumps and turn off the pump. Open the valve to the condenser (V2b). The system is at the end of Step 4, active desorption, at this moment. Do not forget to start data recording in the data acquisition system.
6. Start the Step 1, isolated adsorption, by closing valve to the condenser (V2a) and switch to cool air flow.
7. Wait until the pressure in the adsorption channels equals to the evaporator pressure, open the valve to the evaporator (V1). Isolated adsorption step ends and Step 2, active adsorption, starts at the point. Please note that the temperature of the device is still high (30-40ºC) and isolated adsorption step may take less than 1 min depending on the air flow rate.
8. Keep flowing cooling through the air flow channels. Wait until the set period elapsed, close the valve to the evaporator (V1). Active adsorption step ends at

this point. In this research, the time of adsorption stage (Isolated and active adsorption steps) is set to 30 min.

9. Start step3, isolated desorption, by switching to hot air flow mode.
10. Wait until the pressure in the adsorption channels reaches the condenser pressure, open the valve to the condenser (V2a). Isolated desorption step ends and Step 4, active desorption, starts at this point. Isolated desorption step might take 1 min or less depending on air flow rate. Also, the tube connecting the device and condenser together must be heated to the temperature above the condenser temperature to avoid undesired condensation inside the tube.
11. Wait until the temperature of the device reaches the steady point or the specified time has elapsed, close the valve to the condenser. Active desorption ends.
12. Repeat step 6-11 for the next adsorption desorption cycle.

Appendix B - Tabular Data

Adsorption Isotherm

Table B.1 Equilibrium water uptake when exposed to saturated water vapor.

T(°C)	Weight of dry silica + water + aluminum (g)	Weight of dry silica + aluminum (g)	Weight of dry silica (g)	Weight of water (g)	Equilibrium water uptake (g water/g silica gel)
10	0.3682	0.3088	0.0839	0.0594	0.708
11	0.3659	0.3088	0.0839	0.0571	0.681
13	0.3773	0.3183	0.0865	0.0590	0.682
22	0.3556	0.3088	0.0839	0.0468	0.558
29	0.3606	0.3183	0.0865	0.0423	0.489
33	0.3435	0.3088	0.0839	0.0347	0.414
37	0.3581	0.3183	0.0865	0.0398	0.460
44	0.3404	0.3088	0.0839	0.0316	0.377
47	0.3491	0.3183	0.0865	0.0308	0.356
50	0.3427	0.3183	0.0865	0.0244	0.282
57	0.3431	0.3183	0.0865	0.0248	0.287
63	0.3301	0.3088	0.0839	0.0213	0.254
68	0.3399	0.3183	0.0865	0.0216	0.250
71	0.3259	0.3088	0.0839	0.0171	0.204
75	0.3372	0.3183	0.0865	0.0189	0.218

Table B.2 Equilibrium water uptake when exposed to superheated water vapor.

T(°C)	P (torr)	Psat (Torr)	Weight (g)	Water adsorbed (g)	Water uptake (g water/g silica gel)
36	22.36	44.58	44.7249	0.0919	0.0930
43	22.36	64.84	44.6935	0.0605	0.0612
50	22.36	92.57	44.6764	0.0434	0.0439
57	22.36	129.89	44.6627	0.0297	0.0301
63	22.36	171.44	44.6558	0.0228	0.0231
69	22.36	223.78	44.6507	0.0177	0.0179
71	22.36	243.99	44.6488	0.0158	0.0160
75	22.36	289.07	44.6455	0.0125	0.0126

Adsorption Rate

Table B.3 Water uptake vs. time at 23°C.

Time (min)	Device Weight (g)	Water uptake (g water/g silica gel)
0	41.9598	0
5	42.0125	0.160
5	42.0358	0.231
5	42.0429	0.252
5	42.0181	0.177
5	42.0251	0.198
10	42.0703	0.335
10	42.0836	0.376
10	42.0807	0.367
10	42.0857	0.382
20	42.1243	0.499
20	42.1167	0.476
20	42.1248	0.501
30	42.1664	0.627
30	42.1633	0.618
40	42.1562	0.596
60	42.1655	0.624

Table B.4 Water uptake vs. time at 30°C.

Time (min)	Device Weight (g)	Water uptake (g water/g silica gel)
0	41.9598	0
2	42.0120	0.158
2	42.0174	0.175
2	42.0193	0.181
2	42.0254	0.199
2	42.0292	0.211
5	42.0392	0.241
5	42.0671	0.326
5	42.1015	0.430
5	42.0854	0.381
5	42.0922	0.402
10	42.0669	0.325
10	42.0972	0.417
10	42.0991	0.423
15	42.1107	0.458
20	42.1170	0.477
25	42.1133	0.466
30	42.1071	0.447
90	42.1118	0.461

Table B.5 Water uptake vs. time at 40°C.

Time (min)	Device Weight (g)	Water uptake (g water/g silica gel)
0	61.8619	0
1	61.9610	0.100
1	62.0175	0.157
1	61.9822	0.122
1	61.9999	0.140
3	62.0705	0.211
3	62.0917	0.233
3	62.1067	0.248
3	62.0856	0.226
5	62.1104	0.251
5	62.1302	0.272
5	62.1207	0.262
10	62.1530	0.295
10	62.1288	0.270
10	62.1515	0.293
15	62.1559	0.298
20	62.1631	0.305
25	62.1499	0.291
30	62.1505	0.292
40	62.1711	0.313
180	62.1645	0.306

Base Case Adsorption/Desorption Cycles on Single-Layer Device

Table B.6 Pressure-temperature profiles. (Base Case, single-layer)

Time (min)	T_1 (°C)	T_2 (°C)	T_3 (°C)	dT_3/dt (°C/min)	T_{ev} (°C)	T_{cd} (°C)	P_1 (torr)	P_2 (torr)
0	70.8	59.7	64.5		22.6	30.7	34.96	508
1	36.7	51.8	59.2	-9.0	22.6	30.6	18.93	515
2	30.9	44.8	51.7	-6.0	22.6	30.5	22.89	498
3	28.3	39.7	45.3	-9.0	22.6	30.5	21.92	493
4	26.8	35.7	40.5	-3.0	22.6	30.4	20.86	500
5	25.8	33.2	36.8	0.0	22.6	30.4	21.92	503
6	24.9	31.0	34.0	-3.0	22.5	30.3	21.92	502
7	24.2	29.5	31.9	0.0	22.4	30.3	25.88	487
8	23.9	28.3	30.3	0.0	22.4	30.2	22.89	487
9	23.5	27.3	29.1	-3.0	22.4	30.1	21.92	483
10	23.2	26.7	28.1	0.0	22.3	30.1	20.86	480
11	22.9	26.1	27.3	0.0	22.3	30.0	21.92	485
12	22.7	25.4	26.6	0.0	22.2	30.0	20.86	485
13	22.5	25.1	26.0	-3.0	22.2	29.9	20.86	497
14	22.2	24.7	25.5	0.0	22.1	29.9	19.89	508
15	22.1	24.4	25.1	0.0	22.0	29.8	20.86	510
16	21.9	24.1	24.7	0.0	22.0	29.8	17.87	509
17	21.8	23.8	24.4	0.0	22.0	29.8	20.86	503
18	21.8	23.7	24.1	0.0	22.0	29.8	19.89	497
19	21.6	23.4	23.7	0.0	21.8	29.7	20.86	493
20	21.4	22.9	23.4	0.0	21.7	29.7	20.86	490
21	21.3	22.8	23.1	0.0	21.7	29.7	19.89	492
22	21.1	22.6	22.8	0.0	21.7	29.6	20.86	500
23	21.1	22.4	22.6	0.0	21.6	29.6	20.86	509
24	20.9	22.2	22.3	0.0	21.5	29.6	19.89	510
25	20.9	22.1	22.1	0.0	21.5	29.6	19.89	509
26	20.8	22.0	21.9	-3.0	21.5	29.6	19.89	499
27	20.7	21.8	21.7	0.0	21.4	29.5	20.86	491
28	20.7	21.6	21.5	0.0	21.4	29.5	19.89	484
29	20.6	21.5	21.4	0.0	21.3	29.5	18.93	478
30	20.6	21.3	21.2	0.0	21.3	29.5	20.86	482
31	43.1	25.0	25.0	6.0	21.2	29.5	23.95	499
32	55.3	31.9	32.5	12.0	21.1	29.5	29.94	520
33	60.0	35.5	37.3	3.0	21.1	29.5	34.96	526
34	62.6	37.5	39.7	0.0	21.0	29.5	34.96	518
35	64.6	41.4	43.5	3.0	21.0	29.5	34.96	515
36	66.0	45.5	48.3	6.0	21.0	29.5	33.90	507

Table B.6 Pressure-temperature profiles. (Base Case, single-layer) (Continued)

Time (min)	T_1 (°C)	T_2 (°C)	T_3 (°C)	dT_3/dt (°C/min)	T_{ev} (°C)	T_{cd} (°C)	P_1 (torr)	P_2 (torr)
37	66.9	48.5	51.7	3.0	21.0	29.5	32.93	504
38	67.6	50.5	54.2	0.0	21.0	29.5	34.96	521
39	68.5	52.1	56.0	3.0	21.0	29.4	33.90	528
40	69.4	53.2	57.4	3.0	21.0	29.4	34.96	532
41	70.0	54.2	58.5	0.0	21.0	29.5	35.92	538
42	69.9	54.9	59.4	3.0	21.1	29.5	34.96	543
43	69.6	55.1	60.0	0.0	21.1	29.5	33.90	539
44	69.4	55.3	60.2	0.0	21.1	29.5	34.96	532
45	69.2	55.5	60.4	0.0	21.1	29.5	33.90	524
46	53.2	53.1	60.2	0.0	21.3	29.5	31.96	526
47	31.5	45.8	53.7	-3.0	21.3	29.6	21.92	517
48	26.9	39.3	46.2	-3.0	21.3	29.6	22.89	506
49	24.5	34.3	39.9	-6.0	21.2	29.5	22.89	504
50	23.2	31.0	35.2	-6.0	21.1	29.5	18.93	504
51	22.3	28.3	31.7	-6.0	21.0	29.4	19.89	500
52	21.6	26.7	29.3	0.0	21.0	29.4	20.86	496
53	21.1	25.4	27.5	-3.0	20.9	29.4	19.89	490
54	20.7	24.3	26.1	0.0	20.8	29.3	20.86	486
55	20.4	23.7	25.1	0.0	20.7	29.3	20.86	487
56	20.1	23.1	24.2	0.0	20.6	29.2	20.86	495
57	19.9	22.5	23.5	0.0	20.5	29.2	21.92	487
58	19.6	22.2	22.9	0.0	20.3	29.2	19.89	486
59	19.4	21.8	22.4	0.0	20.2	29.1	19.89	489
60	19.2	21.5	22.0	0.0	20.1	29.1	18.93	493
61	19.1	21.2	21.6	0.0	20.0	29.1	17.87	489
62	19.0	20.8	21.2	0.0	19.9	29.1	19.89	482
63	18.8	20.5	20.8	0.0	19.7	29.1	17.87	478
64	18.7	20.0	20.5	0.0	19.7	29.1	18.93	481
65	18.5	19.9	20.1	0.0	19.6	29.1	19.89	477
66	18.4	19.6	19.8	0.0	19.5	29.1	17.87	470
67	18.3	19.3	19.5	0.0	19.3	29.1	17.87	479
68	18.1	19.1	19.2	0.0	19.2	29.1	17.87	486
69	18.1	18.8	18.9	0.0	19.1	29.0	17.87	485
70	18.1	18.9	18.7	-3.0	19.1	29.1	18.93	483
71	18.0	18.5	18.6	0.0	18.9	29.0	17.87	477
72	17.9	18.3	18.4	0.0	18.8	29.0	17.87	480
73	17.8	18.4	18.3	0.0	18.8	29.1	16.90	484
74	17.8	18.3	18.1	0.0	18.7	29.1	17.87	477
75	17.8	18.3	18.0	0.0	18.7	29.1	17.87	476

Table B.6 Pressure-temperature profiles. (Base Case, single-layer) (Continued)

Time (min)	T_1 (°C)	T_2 (°C)	T_3 (°C)	dT_3/dt (°C/min)	T_{ev} (°C)	T_{cd} (°C)	P_1 (torr)	P_2 (torr)
76	17.7	18.0	17.9	0.0	18.7	29.1	17.87	486
77	43.1	23.5	23.6	6.0	18.6	29.1	24.91	505
78	52.9	30.5	30.8	9.0	18.7	29.2	36.89	516
79	56.9	33.6	35.5	0.0	18.7	29.2	35.92	512
80	59.4	34.9	37.9	3.0	18.8	29.4	37.95	513
81	61.2	36.9	39.7	3.0	18.9	29.5	36.89	520
82	62.9	40.9	43.4	6.0	18.9	29.5	34.96	524
83	64.1	44.6	47.6	3.0	19.0	29.6	35.92	519
84	65.2	47.0	50.7	0.0	19.1	29.6	37.95	519
85	66.5	49.3	53.1	3.0	19.2	29.7	36.89	528
86	67.2	50.9	55.0	3.0	19.3	29.8	35.92	531
87	67.5	52.0	56.4	3.0	19.4	29.9	36.89	536
88	67.9	52.7	57.3	0.0	19.5	30.0	34.96	529
89	68.0	53.5	58.0	0.0	19.6	30.0	34.96	528
90	68.0	53.7	58.6	0.0	19.7	30.1	36.89	528
91	68.0	54.0	59.0	0.0	19.8	30.1	35.92	518
92	68.2	54.1	59.2	0.0	19.8	30.1	34.96	523
93	33.5	47.5	55.5	-6.0	19.9	30.1	24.91	519
94	26.9	40.6	47.6	-9.0	20.0	30.1	20.86	509
95	24.3	35.0	41.0	-6.0	20.1	30.2	20.86	499
96	22.5	30.9	35.8	-3.0	19.9	30.1	20.86	494
97	21.3	28.3	31.9	-3.0	19.9	30.0	17.87	495
98	20.6	26.1	29.1	-3.0	19.8	30.0	18.93	499
99	20.0	24.6	27.0	0.0	19.7	29.9	17.87	487
100	19.6	23.4	25.4	0.0	19.6	29.8	22.89	487
101	19.2	22.8	24.3	0.0	19.6	29.8	17.87	490
102	19.0	21.9	23.4	0.0	19.5	29.8	18.93	490
103	18.8	21.6	22.7	0.0	19.4	29.7	15.93	488
104	18.6	21.3	22.1	0.0	19.4	29.7	15.93	481
105	18.5	20.7	21.6	3.0	19.2	29.6	17.87	482
106	18.3	20.6	21.1	0.0	19.2	29.6	17.87	480
107	18.3	20.3	20.8	-3.0	19.1	29.6	17.87	483
108	18.2	20.2	20.5	0.0	19.1	29.6	17.87	487
109	18.1	19.7	20.2	-3.0	19.0	29.7	17.87	482
110	18.0	19.6	19.9	0.0	18.9	29.6	17.87	486
111	18.0	19.4	19.7	0.0	18.9	29.7	16.90	487
112	18.0	19.3	19.4	0.0	18.8	29.7	16.90	480
113	17.9	19.0	19.2	0.0	18.8	29.7	17.87	481
114	17.9	19.1	19.1	0.0	18.8	29.7	15.93	481

Table B.6 Pressure-temperature profiles. (Base Case, single-layer) (Continued)

Time (min)	T_1 (°C)	T_2 (°C)	T_3 (°C)	dT_3/dt (°C/min)	T_{ev} (°C)	T_{cd} (°C)	P_1 (torr)	P_2 (torr)
115	17.8	18.9	18.9	0.0	18.7	29.7	16.90	483
116	17.8	18.5	18.7	0.0	18.7	29.8	17.87	486
117	17.7	18.5	18.4	0.0	18.5	29.6	17.87	480
118	17.6	18.4	18.2	0.0	18.5	29.6	17.87	483
119	17.5	18.0	18.1	0.0	18.4	29.6	17.87	481
120	17.5	18.1	18.0	0.0	18.4	29.6	16.90	478
121	17.5	18.1	17.9	0.0	18.3	29.6	17.87	484
122	17.5	18.1	17.8	0.0	18.3	29.7	16.90	485
123	35.7	20.9	21.0	6.0	18.2	29.7	18.93	486
124	49.6	28.0	28.1	9.0	18.2	29.7	30.90	491
125	55.6	33.4	34.7	3.0	18.3	29.7	33.90	512
126	58.7	35.3	37.8	3.0	18.3	29.8	35.92	517
127	60.6	37.2	39.8	3.0	18.4	29.9	36.89	518
128	62.1	40.2	42.9	3.0	18.4	29.9	34.96	517
129	63.6	44.5	47.2	0.0	18.5	30.0	34.96	521
130	64.7	46.9	50.6	0.0	18.5	30.0	35.92	523
131	65.5	49.1	53.0	3.0	18.7	30.1	35.92	515
132	66.3	50.7	54.8	0.0	18.7	30.1	34.96	524
133	66.5	51.6	56.1	0.0	18.7	30.1	34.96	525
134	66.6	52.3	57.1	0.0	18.8	30.1	32.93	520
135	67.0	53.4	57.8	0.0	18.9	30.2	36.89	525
136	66.8	53.4	58.4	0.0	19.0	30.2	35.92	524
137	66.9	54.0	58.7	0.0	19.1	30.2	34.96	527
138	53.7	52.4	58.7	-3.0	19.9	30.2	33.90	517
139	30.1	44.7	52.5	-9.0	19.9	30.3	17.87	511
140	25.3	38.4	44.9	-9.0	20.1	30.4	17.87	510
141	23.3	33.5	38.9	-3.0	20.1	30.3	17.87	505
142	21.8	29.9	34.2	-3.0	19.9	30.3	19.89	490
143	20.9	27.4	30.8	-3.0	19.9	30.2	19.89	493
144	20.2	25.6	28.3	0.0	19.9	30.1	17.87	490
145	19.8	24.3	26.5	0.0	19.9	30.1	18.93	482
146	19.5	23.2	25.1	0.0	19.9	30.1	17.87	490
147	19.0	22.4	24.0	0.0	19.7	30.0	17.87	486
148	18.7	21.5	23.0	-3.0	19.6	30.0	16.90	488
149	18.5	21.3	22.2	0.0	19.4	29.9	16.90	487
150	18.3	20.7	21.7	0.0	19.4	29.9	18.93	481
151	18.2	20.4	21.1	0.0	19.2	29.8	18.93	483
152	18.0	20.0	20.6	0.0	19.2	29.8	18.93	487
153	17.8	19.7	20.2	0.0	19.1	29.8	17.87	485

Table B.6 Pressure-temperature profiles. (Base Case, single-layer) (Continued)

Time (min)	T_1 (°C)	T_2 (°C)	T_3 (°C)	dT_3/dt (°C/min)	T_{ev} (°C)	T_{cd} (°C)	P_1 (torr)	P_2 (torr)
154	17.8	19.6	19.8	0.0	18.9	29.7	17.87	487
155	17.7	19.0	19.5	0.0	18.8	29.7	17.87	479
156	17.5	18.7	19.2	0.0	18.7	29.6	16.90	488
157	17.5	18.5	18.9	0.0	18.7	29.6	17.87	488
158	17.3	18.6	18.6	0.0	18.5	29.6	16.90	479
159	17.3	18.5	18.4	3.0	18.5	29.6	15.93	481
160	17.3	18.1	18.2	0.0	18.4	29.6	15.93	489
161	17.2	18.0	18.0	0.0	18.3	29.6	17.87	484
162	17.2	17.8	17.8	0.0	18.3	29.6	17.87	482
163	17.1	17.7	17.6	0.0	18.2	29.5	17.87	483
164	17.1	17.5	17.5	0.0	18.1	29.5	17.87	487
165	17.1	17.5	17.3	0.0	18.1	29.5	16.90	482
166	17.1	17.3	17.3	0.0	18.1	29.6	16.90	479
167	17.0	17.2	17.2	-3.0	18.1	29.6	16.90	477
168	17.0	17.1	17.0	0.0	18.0	29.6	16.90	477
169	42.6	22.7	22.5	3.0	17.9	29.6	20.86	503
170	51.7	29.9	29.9	6.0	17.9	29.6	33.90	502
171	56.1	34.7	36.3	6.0	18.0	29.6	37.95	512
172	58.6	36.4	38.7	3.0	18.0	29.7	35.92	511
173	60.3	38.5	41.1	3.0	18.1	29.8	36.89	514
174	61.8	42.5	44.9	6.0	18.2	29.9	36.89	512
175	63.5	45.2	48.5	3.0	18.3	30.0	38.92	516
176	64.2	47.4	51.2	3.0	18.3	30.0	35.92	527
177	64.4	48.9	53.1	0.0	18.3	30.0	36.89	523
178	64.4	50.3	54.4	0.0	18.4	30.0	36.89	518
179	64.7	50.8	55.3	0.0	18.5	30.1	35.92	519
180	65.2	51.5	56.1	3.0	18.5	30.1	35.92	530
181	65.2	52.4	56.7	0.0	18.7	30.2	36.89	527
182	65.4	52.5	57.2	3.0	18.7	30.2	36.89	519
183	65.5	52.6	57.5	3.0	18.8	30.3	36.89	526

Table B.7 Heat transfer vs. time calculation. (Base Case, single-layer)

Time	1st Desorption Cycle				2nd Desorption Cycle			
(min)	T_1 (°C)	T_2 (°C)	q (W)	Q_{acc} (J)	T_1 (°C)	T_2 (°C)	q (W)	Q_{acc} (J)
0	20.6	21.3		0	17.7	18.0		0
0.5	40.9	24.5	2.4	44	37.6	21.2	2.4	41
1.0	49.8	28.1	3.2	130	45.7	25.0	3.0	125
1.5	54.7	31.4	3.4	229	50.6	28.3	3.3	220
2.0	57.7	34.0	3.5	332	53.9	31.1	3.3	318
2.5	59.8	35.4	3.6	438	56.0	32.8	3.4	419
3.0	61.2	36.5	3.6	546	57.4	34.1	3.4	521
3.5	62.4	37.3	3.7	656	58.6	34.7	3.5	625
4.0	63.4	38.7	3.6	765	59.7	35.4	3.6	731
4.5	64.4	41.1	3.4	870	60.5	36.2	3.5	837
5.0	65.3	43.5	3.2	969	61.5	37.2	3.6	943
5.5	66.0	45.4	3.0	1063	62.3	39.2	3.4	1048
6.0	66.3	46.7	2.9	1151	63.2	41.4	3.2	1146
6.5	66.8	48.2	2.7	1234	63.9	43.4	3.0	1239
7.0	67.2	49.5	2.6	1314	64.2	45.0	2.8	1326
7.5	67.6	50.3	2.5	1390	64.7	46.3	2.7	1408
8.0	68.2	51.2	2.5	1465	65.4	48.0	2.5	1487
8.5	68.4	51.9	2.4	1539	66.1	48.5	2.6	1564
9.0	68.8	52.6	2.4	1611	66.7	49.4	2.5	1640
9.5	69.3	52.9	2.4	1682	67.1	50.6	2.4	1714
10.0	69.6	53.4	2.4	1753	67.2	51.0	2.4	1785
10.5	69.9	54.2	2.3	1823	67.5	51.6	2.3	1855
11.0	70.0	54.5	2.3	1891	67.5	51.9	2.3	1923
11.5	69.9	54.9	2.2	1959	67.6	52.3	2.2	1991
12.0	69.9	54.9	2.2	2025	67.9	53.0	2.2	2057
12.5	69.7	54.9	2.2	2089	67.9	53.2	2.1	2123
13.0	69.5	55.2	2.1	2152	68.0	53.7	2.1	2187
13.5	69.4	55.3	2.1	2214	67.9	53.8	2.1	2250
14.0	69.4	55.5	2.0	2275	68.0	53.8	2.1	2313
14.5	69.2	55.4	2.0	2337	67.9	53.8	2.1	2375
15.0	69.1	55.4	2.0	2397	68.1	54.3	2.0	2437

Table B.7 Heat transfer vs. time calculation. (Base Case, single-layer) (Continued)

Time	3rd Desorption Cycle				4th Desorption Cycle			
(min)	T_1 (°C)	T_2 (°C)	q (W)	Q_{acc} (J)	T_1 (°C)	T_2 (°C)	q (W)	Q_{acc} (J)
0	17.5	18.0		0	17.0	17.1		0
0.5	37.0	21.2	2.3	41	36.0	20.1	2.3	43
1.0	45.2	24.7	3.0	123	44.2	23.6	3.0	126
1.5	50.0	28.2	3.2	215	49.0	27.4	3.2	219
2.0	53.4	31.5	3.2	312	52.4	30.4	3.2	315
2.5	55.8	33.6	3.2	408	54.8	33.1	3.2	411
3.0	57.4	34.5	3.3	506	56.4	35.5	3.1	504
3.5	58.8	35.4	3.4	607	57.6	35.8	3.2	598
4.0	59.9	36.8	3.4	709	58.9	36.6	3.3	694
4.5	60.6	37.4	3.4	810	59.9	37.5	3.3	792
5.0	61.4	38.4	3.4	911	60.4	38.9	3.1	888
5.5	62.2	40.7	3.1	1010	61.2	41.0	2.9	980
6.0	63.0	42.7	3.0	1102	62.0	42.6	2.8	1065
6.5	63.7	44.8	2.8	1188	63.1	44.3	2.7	1149
7.0	64.2	46.3	2.6	1269	63.5	45.9	2.6	1229
7.5	64.7	47.1	2.6	1347	63.9	46.9	2.5	1306
8.0	65.1	48.3	2.5	1422	64.2	47.6	2.4	1379
8.5	65.5	49.5	2.3	1495	64.2	48.7	2.3	1449
9.0	66.0	50.0	2.3	1564	64.3	49.1	2.2	1517
9.5	66.3	50.8	2.3	1634	64.3	49.9	2.1	1581
10.0	66.5	51.2	2.2	1702	64.5	50.3	2.1	1643
10.5	66.5	51.7	2.2	1767	64.7	50.8	2.0	1704
11.0	66.6	52.8	2.0	1830	64.7	51.3	2.0	1765
11.5	66.7	52.5	2.1	1891	64.9	51.7	1.9	1824
12.0	66.9	53.2	2.0	1953	65.2	51.5	2.0	1883
12.5	67.0	53.0	2.0	2012	65.1	51.7	2.0	1940
13.0	67.0	53.3	2.0	2073	65.3	52.2	1.9	1998
13.5	66.8	53.3	2.0	2132	65.4	52.5	1.9	2053
14.0	66.9	53.6	1.9	2191	65.4	52.4	1.9	2110
14.5	66.9	54.2	1.9	2248	65.4	52.5	1.9	2165
15.0	66.9	54.1	1.9	2305	65.4	52.6	1.9	2221

Base Case Adsorption/Desorption Cycles on Three-Layer Device

Table B.8 Pressure-temperature profiles. (Base Case, three-layer)

Time (min)	T_1 (°C)	T_2 (°C)	T_3 (°C)	dT_3/dt (°C/min)	T_{ev} (°C)	T_{cd} (°C)	P_1 (torr)	P_2 (torr)
0	60.0	58.6	57.4	0.00	23.1	30.0	32.54	1842
1	33.1	46.8	47.1	-12.67	23.1	29.9	18.79	1044
2	27.2	36.5	37.2	-7.33	23.1	30.0	18.45	1062
3	25.1	31.1	31.8	-4.00	23.1	30.0	15.62	1071
4	24.3	28.5	29.0	-2.00	23.1	29.9	15.06	1096
5	24.1	27.2	27.5	-1.33	23.0	29.9	14.84	1077
6	23.9	26.6	26.7	0.00	22.9	29.9	16.17	1064
7	24.1	26.2	26.2	0.00	22.9	29.9	15.61	1045
8	24.1	25.9	25.9	0.00	22.8	29.9	17.54	1045
9	24.0	25.7	25.6	0.00	22.7	29.8	15.50	1007
10	23.9	25.4	25.3	-0.67	22.5	29.8	17.18	992
11	23.6	25.2	25.1	0.00	22.5	29.8	16.50	1010
12	23.4	24.9	24.8	0.00	22.4	29.8	17.13	1034
13	23.3	24.8	24.6	0.00	22.4	29.8	17.55	1053
14	23.2	24.6	24.4	0.00	22.4	29.7	17.43	1059
15	23.2	24.4	24.2	0.00	22.3	29.7	17.06	1097
16	23.1	24.3	24.1	0.00	22.3	29.7	16.74	1088
17	23.0	24.2	24.0	0.00	22.2	29.7	16.94	1086
18	23.0	24.1	23.9	0.00	22.1	29.7	16.29	1059
19	23.0	24.0	23.9	-0.67	22.1	29.7	16.50	1056
20	23.0	23.9	23.8	0.00	22.0	29.7	17.76	1017
21	23.0	23.9	23.7	0.00	22.0	29.6	17.55	978
22	23.0	23.9	23.6	-0.67	22.0	29.6	17.29	998
23	23.0	23.8	23.6	0.00	22.0	29.6	17.77	980
24	23.0	23.8	23.5	0.00	22.0	29.7	17.54	985
25	23.0	23.7	23.5	0.00	21.9	29.7	17.28	1001
26	23.0	23.7	23.5	0.00	22.0	29.7	16.73	1049
27	23.0	23.6	23.4	0.00	22.0	29.7	17.30	1085
28	23.0	23.5	23.4	0.00	21.9	29.7	17.66	1089
29	23.0	23.5	23.3	0.00	21.9	29.6	17.88	1087
30	22.9	23.4	23.3	0.00	21.8	29.6	17.89	1057
31	40.0	27.6	26.3	12.00	21.8	29.6	24.11	1917
32	51.5	37.0	35.9	5.33	21.9	29.7	33.04	1856
33	55.5	40.5	39.9	4.00	22.0	29.8	37.00	1845
34	57.8	44.0	43.4	4.00	22.0	29.8	36.71	1869
35	59.3	50.7	48.7	5.33	22.0	29.8	33.37	1849
36	59.8	55.0	53.0	3.33	22.0	29.8	33.58	1908

Table B.8 Pressure-temperature profiles. (Base Case, three-layer) (Continued)

Time (min)	T_1 (°C)	T_2 (°C)	T_3 (°C)	dT_3/dt (°C/min)	T_{ev} (°C)	T_{cd} (°C)	P_1 (torr)	P_2 (torr)
37	59.8	57.0	55.1	1.33	22.1	29.9	34.07	1979
38	59.7	57.5	56.7	2.00	22.2	29.9	34.45	2050
39	47.0	55.5	54.5	-6.67	22.2	29.9	29.63	1048
40	29.8	41.9	43.2	-10.67	22.2	29.9	16.75	1048
41	26.2	33.8	35.5	-6.00	22.2	29.9	17.06	1033
42	24.7	29.8	31.0	-3.33	22.2	29.9	16.39	1023
43	24.1	27.8	28.6	-2.00	22.2	29.8	17.18	1003
44	23.7	26.7	27.3	-1.33	22.1	29.8	16.85	966
45	23.5	26.1	26.4	-0.67	22.1	29.8	17.66	933
46	23.4	25.6	25.8	-0.67	22.0	29.8	17.53	941
47	23.3	25.3	25.4	0.00	22.0	29.8	16.64	932
48	23.4	25.1	24.9	-0.67	22.0	29.8	17.30	942
49	23.3	24.9	24.7	0.00	21.9	29.8	17.10	971
50	23.2	24.7	24.5	0.00	21.7	29.8	17.65	1018
51	23.2	24.5	24.3	0.00	21.8	29.8	17.66	1053
52	23.1	24.4	24.2	0.00	21.7	29.8	17.43	1039
53	23.1	24.3	24.0	0.00	21.8	29.8	16.41	1014
54	23.0	24.2	24.0	0.00	21.7	29.8	17.66	988
55	23.0	24.2	23.9	0.00	21.7	29.8	17.06	980
56	23.0	24.0	23.8	0.00	21.7	29.8	16.62	950
57	22.9	23.9	23.7	0.00	21.7	29.8	15.62	926
58	22.9	23.9	23.6	0.00	21.7	29.8	16.86	939
59	22.9	23.9	23.6	0.00	21.6	29.8	17.19	935
60	22.9	23.8	23.5	0.00	21.6	29.8	16.40	954
61	22.9	23.8	23.5	0.00	21.6	29.8	17.78	976
62	23.0	23.7	23.4	0.00	21.6	29.8	18.23	1024
63	23.0	23.7	23.4	0.00	21.5	29.8	17.41	1050
64	22.9	23.6	23.4	0.00	21.5	29.8	17.55	1045
65	23.0	23.6	23.4	0.00	21.5	29.8	17.77	1021
66	22.9	23.5	23.3	-0.67	21.5	29.8	18.80	1011
67	22.9	23.5	23.3	0.00	21.5	29.8	18.00	1000
68	22.9	23.5	23.3	0.00	21.5	29.8	18.21	1000
69	22.9	23.5	23.3	0.00	21.5	29.8	17.31	966
70	48.9	34.1	32.8	12.67	21.5	29.8	32.24	1902
71	55.0	39.8	39.5	4.67	21.5	29.8	36.77	1921
72	56.9	42.6	44.3	2.67	21.6	29.8	38.92	1968
73	59.1	48.2	49.0	6.67	21.6	29.8	36.42	1999
74	59.9	53.6	53.9	3.33	21.7	29.8	35.61	2011
75	60.1	56.4	56.4	2.00	21.7	29.9	35.39	2077

Table B.8 Pressure-temperature profiles. (Base Case, three-layer) (Continued)

Time (min)	T_1 (°C)	T_2 (°C)	T_3 (°C)	dT_3/dt (°C/min)	T_{ev} (°C)	T_{cd} (°C)	P_1 (torr)	P_2 (torr)
76	60.3	57.8	57.8	1.33	21.8	29.9	35.09	2056
77	60.4	58.5	58.4	0.67	21.9	30.0	34.54	2047
78	35.7	52.8	50.2	-14.67	22.0	30.0	21.95	992
79	27.9	41.1	39.2	-8.00	22.0	30.0	17.55	988
80	25.5	34.4	33.1	-4.67	22.0	30.0	17.13	981
81	24.4	30.5	29.7	-2.67	21.9	30.0	17.88	953
82	23.9	28.5	27.9	-1.33	21.9	30.0	17.65	938
83	23.6	27.4	26.8	-1.33	21.8	30.0	16.27	927
84	23.4	26.6	26.1	-1.33	21.8	29.9	15.84	936
85	23.3	26.0	25.6	0.00	21.7	29.9	18.00	953
86	23.2	25.6	25.2	0.00	21.6	29.8	17.54	970
87	23.2	25.3	24.9	0.00	21.6	29.8	18.22	986
88	23.2	25.0	24.7	0.00	21.5	29.8	18.47	1000
89	23.1	24.8	24.5	0.00	21.5	29.8	18.23	1005
90	23.1	24.7	24.4	0.00	21.5	29.8	16.62	988
91	23.0	24.5	24.2	0.00	21.5	29.8	17.19	980
92	23.0	24.4	24.1	0.00	21.4	29.8	17.31	972
93	23.0	24.3	24.0	0.00	21.4	29.8	16.19	967
94	23.0	24.2	23.9	0.00	21.3	29.7	17.41	959
95	22.9	24.1	23.8	0.00	21.3	29.7	18.93	954
96	22.9	24.0	23.8	-0.67	21.2	29.6	18.11	978
97	22.9	23.9	23.7	0.00	21.2	29.6	17.98	994
98	23.0	23.8	23.6	0.00	21.2	29.6	18.22	1005
99	22.9	23.8	23.5	0.00	21.2	29.6	18.32	1011
100	22.9	23.8	23.5	0.00	21.2	29.6	18.11	1031
101	22.9	23.7	23.5	0.00	21.1	29.6	18.41	1023
102	22.9	23.6	23.4	0.00	21.1	29.6	18.44	1003
103	22.8	23.5	23.4	0.00	21.1	29.6	18.67	995
104	22.8	23.5	23.3	0.00	21.1	29.6	18.78	982
105	22.8	23.4	23.3	0.00	21.1	29.6	18.34	1000
106	22.8	23.4	23.3	0.00	21.1	29.6	17.65	983
107	22.8	23.4	23.2	0.00	21.1	29.6	16.62	967
108	31.1	24.2	24.8	12.67	21.1	29.6	19.03	1902
109	50.7	35.1	36.8	8.00	21.2	29.7	34.52	1950
110	55.5	39.3	41.5	3.33	21.3	29.7	37.33	1952
111	57.9	42.7	45.0	3.33	21.3	29.7	38.69	1923
112	59.4	49.0	50.1	5.33	21.4	29.8	37.12	1950
113	59.9	54.0	54.4	3.33	21.5	29.8	36.18	1962
114	60.0	56.4	56.6	1.33	21.5	29.8	35.75	1936

Table B.8 Pressure-temperature profiles. (Base Case, three-layer) (Continued)

Time (min)	T_1 (°C)	T_2 (°C)	T_3 (°C)	dT_3/dt (°C/min)	T_{ev} (°C)	T_{cd} (°C)	P_1 (torr)	P_2 (torr)
115	60.0	57.6	57.6	0.67	21.5	29.8	35.63	1918

Table B.9 Heat transfer vs. time calculation (Base Case, three-layer)

Time (min)	1st Desorption Cycle				2nd Desorption Cycle			
	T_1 (°C)	T_2 (°C)	q (W)	Q_{acc} (J)	T_1 (°C)	T_2 (°C)	q (W)	Q_{acc} (J)
0	43.3	29.8	9.1	200	45.5	30.4	10.1	223
0.5	49.3	35.2	9.5	482	51.1	36.1	10.1	523
1.0	52.2	37.7	9.7	772	54.0	38.6	10.3	832
1.5	54.3	39.5	9.9	1068	55.6	40.6	10.1	1139
2.0	55.9	41.0	10.0	1369	56.4	41.9	9.7	1439
2.5	57.2	42.6	9.8	1667	57.2	43.4	9.3	1727
3.0	58.1	44.6	9.1	1951	58.6	46.1	8.4	1995
3.5	58.8	48.1	7.2	2194	59.4	49.7	6.5	2217
4.0	59.5	51.6	5.3	2379	59.9	52.5	5.0	2388
4.5	59.6	53.8	3.9	2514	60.0	54.5	3.7	2514
5.0	59.9	55.4	3.0	2615	60.0	55.9	2.8	2609
5.5	59.8	56.4	2.3	2692	60.1	56.8	2.2	2684
6.0	59.9	57.1	1.9	2753	60.2	57.5	1.8	2744
6.5	60.2	57.4	1.9	2811	60.3	58.0	1.5	2793
7.0	59.8	57.6	1.5	2861	60.3	58.4	1.3	2836

Table B.9 Heat transfer vs. time calculation. (Base Case, three-layer) (Continued)

Time (min)	3rd Desorption Cycle			
	T_1 (°C)	T_2 (°C)	q (W)	Q_{acc} (J)
0	23.0	23.4	0	0
0.5	42.4	28.1	9.6	190
1.0	49.2	33.9	10.3	493
1.5	53.2	36.8	11.0	814
2.0	55.0	38.8	10.9	1142
2.5	56.3	40.5	10.6	1465
3.0	57.6	42.1	10.4	1782
3.5	58.5	44.5	9.4	2083
4.0	59.3	47.9	7.7	2339
4.5	59.7	51.1	5.8	2538
5.0	59.8	53.4	4.3	2688
5.5	60.0	55.0	3.4	2801
6.0	60.0	56.2	2.6	2889
6.5	60.0	56.9	2.1	2957
7.0	60.0	57.4	1.7	3013

Appendix C – Calibration Chart of the Flow Meter

Table C.1 Calibration Chart of Matheson Tri-Gas 604 flow meter [28]

Reading scale	Flow rate (SLPM)		
	P=0 torr gauge	P=1034 torr gauge	P=2585 torr gauge
150	16.58	25.72	35.14
149	16.49	25.59	34.96
148	16.39	25.45	34.77
147	16.29	25.31	34.59
146	16.19	25.18	34.40
145	16.09	25.04	34.21
144	15.99	24.89	34.01
143	15.89	24.75	33.82
142	15.79	24.60	33.62
141	15.68	24.46	33.42
140	15.58	24.31	33.21
139	15.47	24.16	33.01
138	15.37	24.01	32.80
137	15.26	23.85	32.59
136	15.15	23.70	32.38
135	15.05	23.54	32.17
134	14.94	23.39	31.95
133	14.83	23.23	31.74
132	14.73	23.07	31.52
131	14.62	22.91	31.30
130	14.51	22.74	31.08
129	14.40	22.58	30.85
128	14.29	22.42	30.63
127	14.19	22.25	30.40
126	14.08	22.08	30.17
125	13.97	21.92	29.94
124	13.86	21.75	29.71
123	13.75	21.58	29.48
122	13.64	21.41	29.25
121	13.54	21.24	29.01
120	13.43	21.06	28.78
119	13.32	20.89	28.54
118	13.21	20.72	28.30
117	13.10	20.54	28.06
116	13.00	20.37	27.82
115	12.89	20.19	27.58

Table C.1 Calibration Chart of Matheson Tri-Gas 604 flow meter (Continued)

Reading scale	Flow rate (SLPM)		
	P=0 torr gauge	P=1034 torr gauge	P=2585 torr gauge
114	12.78	20.01	27.34
113	12.67	19.83	27.10
112	12.57	19.66	26.85
111	12.46	19.48	26.61
110	12.35	19.30	26.36
109	12.24	19.12	26.12
108	12.13	18.94	25.87
107	12.03	18.76	25.62
106	11.92	18.57	25.37
105	11.81	18.39	25.12
104	11.70	18.21	24.87
103	11.59	18.03	24.62
102	11.49	17.84	24.37
101	11.38	17.66	24.12
100	11.27	17.47	23.87
99	11.16	17.29	23.62
98	11.05	17.11	23.36
97	10.94	16.92	23.11
96	10.83	16.73	22.86
95	10.72	16.55	22.61
94	10.61	16.36	22.35
93	10.50	16.18	22.10
92	10.39	15.99	21.84
91	10.28	15.80	21.59
90	10.17	15.62	21.33
89	10.06	15.43	21.08
88	9.95	15.24	20.82
87	9.84	15.06	20.57
86	9.73	14.87	20.31
85	9.61	14.68	20.06
84	9.50	14.50	19.80
83	9.39	14.31	19.55
82	9.28	14.12	19.29
81	9.16	13.94	19.03
80	9.05	13.75	18.78
79	8.94	13.56	18.52
78	8.82	13.37	18.27

Table C.1 Calibration Chart of Matheson Tri-Gas 604 flow meter (Continued)

Reading scale	Flow rate (SLPM)		
	P=0 torr gauge	P=1034 torr gauge	P=2585 torr gauge
77	8.71	13.19	18.01
76	8.59	13.00	17.76
75	8.48	12.81	17.50
74	8.36	12.63	17.25
73	8.25	12.44	16.99
72	8.13	12.25	16.74
71	8.02	12.07	16.48
70	7.90	11.88	16.23
69	7.78	11.69	15.97
68	7.67	11.51	15.72
67	7.55	11.32	15.46
66	7.43	11.14	15.21
65	7.32	10.95	14.96
64	7.20	10.76	14.70
63	7.08	10.58	14.45
62	6.96	10.39	14.20
61	6.85	10.21	13.95
60	6.73	10.02	13.69
59	6.61	9.84	13.44
58	6.49	9.65	13.19
57	6.37	9.47	12.94
56	6.26	9.29	12.69
55	6.14	9.10	12.44
54	6.02	8.92	12.19
53	5.90	8.73	11.93
52	5.79	8.55	11.68
51	5.67	8.37	11.43
50	5.55	8.18	11.19
49	5.43	8.00	10.94
48	5.31	7.82	10.69
47	5.20	7.64	10.44
46	5.08	7.46	10.19
45	4.96	7.27	9.94
44	4.85	7.09	9.69
43	4.73	6.91	9.45
42	4.61	6.73	9.20
41	4.50	6.55	8.95

Table C.1 Calibration Chart of Matheson Tri-Gas 604 flow meter (Continued)

Reading scale	Flow rate (SLPM)		
	P=0 torr gauge	P=1034 torr gauge	P=2585 torr gauge
40	4.38	6.37	8.70
39	4.26	6.19	8.46
38	4.15	6.01	8.21
37	4.03	5.83	7.97
36	3.92	5.64	7.72
35	3.80	5.46	7.47
34	3.69	5.28	7.23
33	3.57	5.11	6.98
32	3.46	4.93	6.74
31	3.34	4.75	6.49
30	3.23	4.57	6.25
29	3.12	4.39	6.00
28	3.00	4.21	5.76
27	2.89	4.03	5.51
26	2.77	3.85	5.27
25	2.66	3.67	5.02
24	2.54	3.49	4.78
23	2.43	3.31	4.54
22	2.32	3.14	4.29
21	2.20	2.96	4.05
20	2.09	2.78	3.80

Appendix D - Derivation of Energy Balance Equation

$$\dot{q} - \dot{q}_{lost} + U_{wv,ev}\dot{m}_{wv,ev} - U_{wv,adsorber}\dot{m}_{wv,cd}$$
$$= \frac{d}{dt}\left(m_{al}U_{al}\right) + \frac{d}{dt}\left(m_{sg}U_{sg}\right) + \frac{d}{dt}\left(m_{wv,adsorber}U_{wv,adsorber}\right) + \frac{d}{dt}\left(m_{wa}U_{wa}\right) \tag{13}$$

$$\dot{q} - \dot{q}_{lost} + U_{wv,ev}\dot{m}_{wv,ev} - U_{wv,adsorber}\dot{m}_{wv,cd}$$
$$= \left(m_{al}C_{v,al} + m_{sg}C_{v,sg} + m_{wv,adsorber}C_{v,wv} + m_{wa}C_{v,wa}\right)\frac{dT}{dt}$$
$$+ U_{wv,adsorber}\frac{d}{dt}\left(m_{wv,adsorber}\right) + U_{wa}\frac{d}{dt}\left(m_{wa}\right)$$

$$\dot{q} - \dot{q}_{lost} + U_{wv,ev}\dot{m}_{wv,ev} - U_{wv,adsorber}\dot{m}_{wv,cd}$$
$$= \left(m_{al}C_{v,al} + m_{sg}C_{v,sg} + m_{wv,adsorber}C_{v,wv} + m_{wa}C_{v,wa}\right)\frac{dT}{dt}$$
$$+ U_{wv,adsorber}\left(\dot{m}_{wv,ev} - \dot{m}_{wv,cd} - r_{adsorption}m_{sg}\right) + U_{wa}r_{adsorption}m_{sg}$$

$$\dot{q} - \dot{q}_{lost} + \left(U_{wv,ev} - U_{wv,adsorber}\right)\dot{m}_{wv,ev} - \left(U_{wa} - U_{wv,adsorber}\right)r_{adsorption}m_{sg}$$
$$= \left(m_{al}C_{v,al} + m_{sg}C_{v,sg} + m_{wv,adsorber}C_{v,wv} + m_{wa}C_{v,wa}\right)\frac{dT}{dt}$$

$$\dot{q} - \dot{q}_{lost} + \left(T_{ev} - T\right)C_{v,wv}\dot{m}_{wv,ev} - r_{adsorption}m_{sg}\Delta U_{adsorption}$$
$$= \left(m_{al}C_{p,al} + m_{sg}C_{p,sg} + \frac{PV}{MW_w RT}C_{v,wv} + Lm_{sg}C_{p,wa}\right)\frac{dT}{dt} \tag{14}$$

Appendix E - Matlab Source Code

Main M-File

```
clc
clear all

global mal msg Cpal Cpsg Cvwv Cpwa Cpair mair MWw R1 R2 V Tev Tcd Troom
Taincool Tainhot dUadsorption dHevap UA UAlost Pev Pcd;

%Define input parameters
tads=1800; %s
tdes=450; %s
tcycle=tads+tdes; %(adsorption+desorption)

%Define constants%
K=273.15; %0C=273.15K
msg=0.9882; %g
mal=39.694; %g
Cpal=0.897; %J/g.K
Cpsg=0.740; %J/g.K
Cvwv=1.4; %J/g.K
Cpwa=4.185; %J/g.K
MWw=18.015; %g/mol
R1=8.314; %J/mol.K
R2=62363.67; %cm^3.Torr/mol.K
V=6.71; %cm^3
Troom=23+K; %C
Taincool=23+K; %c
Tainhot=60+K; %c
Tguess=57.8+K;
Tev=22+K; %C
Tcd=30+K; %C
dUadsorption=-2800; %J/g
dHevap=2442.5; %J/g at 25C
mair=0.644; %g/s
Cpair=1.012; %J/g.K
muair=18.27e-3; %g/m.s
kair=0.02; %W/m.K

%Define Channel dimension%
nol=3; %number of layer
hD=0.016*2.54/100; %m
wD=0.23*2.54/100; %m
lD=1.73*2.54/100; %m
```

```
Dh=2*hD*wD/(hD+wD);
Across=wD*hD; %m^2
Aheat=(nol+1)*6*lD*2*(hD+wD); %m^2
Alost=2*2*2*2.54*2.54/100/100; %m^2

%Flow property%
Re=Dh*mair/(6*(nol+1)*muair*Across);
Pr=Cpair*muair/kair;
Nu=1.86*(Dh*Re*Pr/lD)^(1/3);%
hair=Nu*kair/Dh;
sigmaLK=1.7e-6+6.8e-5+1.7e-7;% m2.K/W
UA=Aheat/(1/hair+sigmaLK);
UAlost=0.07/0.02*Alost; %W/K

Pev=Psat(Tev);
Pcd=Psat(Tcd);

%Y=[P T L Qacc Qacclost]
Y0=[Pcd Tguess Leq(Pcd,Tguess) 0 0]; %Initial condition


options1=odeset('Events',@events1);
[t1,Y1]=ode15s(@Step1,[0 tads],Y0,options1);
dim=size(Y1);
Y1e=Y1(dim(1),:);
Tout1=(Taincool-Y1(:,2))/exp(UA/mair/Cpair)+Y1(:,2);

[t2,Y2]=ode15s(@Step2,[t1(dim(1)) tads],Y1e);
dim=size(Y2);
Y2e=Y2(dim(1),:);
Tout2=(Taincool-Y2(:,2))/exp(UA/mair/Cpair)+Y2(:,2);

Y3i=Y2e;
Y3i(4)=0;
Y3i(5)=0;

options3=odeset('Events',@events3);
[t3,Y3]=ode15s(@Step3,[0 tdes],Y3i,options3);
dim=size(Y3);
Y3e=Y3(dim(1),:);
Tout3=(Tainhot-Y3(:,2))/exp(UA/mair/Cpair)+Y3(:,2);

[t4,Y4]=ode15s(@Step4,[t3(dim(1)) tdes],Y3e);
dim=size(Y4);
```

```
Y4e=Y4(dim(1),:);
Tout4=(Tainhot-Y4(:,2))/exp(UA/mair/Cpair)+Y4(:,2);

T=[Y1(:,2);Y2(:,2);Y3(:,2);Y4(:,2)];
P=[Y1(:,1);Y2(:,1);Y3(:,1);Y4(:,1)];
L=[Y1(:,3);Y2(:,3);Y3(:,3);Y4(:,3)];
Qacc=[Y1(:,4);Y2(:,4);Y3(:,4);Y4(:,4)];
Tout=[Tout1;Tout2;Tout3;Tout4];
t=[t1;t2;t3+tads;t4+tads];

dim=size(t);

for n=1:dim(1)
Lsat(n)=Leq(P(n),T(n));
end;
Lsat=Lsat';

T=T-273.15;
Tout=Tout-273.15;

subplot(2,1,1)
plot(t,P,t,T,t,Tout)

subplot(2,1,2)
plot(t,L,t,Lsat)

mevap=(Y2e(3)-Y4e(3))*msg
COP=mevap*dHevap/Y4e(4)
SCP=(Y2e(3)-Y4e(3))*dHevap/tcycle*1000
```

ODE Function of Step 1, Isolated Adsorption

```
function dy=Step1(t,y)
global mal msg Cpal Cpsg Cvwv Cpwa Cpair mair MWw R2 V Tev Tcd Troom
Taincool Tainhot dUadsorption dHevap UA UAlost
dy=zeros(5,1);
dy(1)=-
radsorption(y(1),y(2),y(3))*msg*MWw*R2*y(2)/V+y(1)/y(2)*(q(Taincool,y(2))-
qlost(y(2),Troom)-
radsorption(y(1),y(2),y(3))*msg*dUadsorption)/(mal*Cpal+msg*Cpsg+y(1)*V/(MW
w*R2*y(2))*Cvwv+y(3)*msg*Cpwa);
```

```
dy(2)=(q(Taincool,y(2))-qlost(y(2),Troom)-
radsorption(y(1),y(2),y(3))*msg*dUadsorption)/(mal*Cpal+msg*Cpsg+y(1)*V/(MW
w*R2*y(2))*Cvwv+y(3)*msg*Cpwa);
dy(3)=radsorption(y(1),y(2),y(3));
dy(4)=q(Taincool,y(2));
dy(5)=qlost(y(2),Troom);
%y=[P Twall L Qacc Qacclost]
```

Event Function to Terminate Step 1

```
function [value,isterminal,direction] = events1(t,y)

global Pev

value = y(1)-Pev ;     % Detect height = 0
isterminal = 1;   % Stop the integration
direction = 0;   % Both direction
```

ODE Function of Step 2, Continued Adsorption

```
function dy=Step2(t,y)
global mal msg Cpal Cpsg Cvwv Cpwa Cpair mair MWw R2 V Tev Tcd Troom
Taincool Tainhot dUadsorption dHevap UA UAlost
dy=zeros(5,1);
dy(1)=0;
dy(2)=(radsorption(y(1),y(2),y(3))*msg+(q(Taincool,y(2))-qlost(y(2),Troom)-
radsorption(y(1),y(2),y(3))*msg*dUadsorption)/((Tev-
y(2))*Cvwv))/((mal*Cpal+msg*Cpsg+y(1)*V/(MWw*R2*y(2))*Cvwv+y(3)*msg*C
pwa)/((Tev-y(2))*Cvwv)-y(1)*V/(MWw*R2*y(2)^2));
dy(3)=radsorption(y(1),y(2),y(3));
dy(4)=q(Taincool,y(2));
dy(5)=qlost(y(2),Troom);
%Y=[P T L Qacc Qacclost]
```

ODE Function of Step 3, Isolated Desorption

```
function dy=Step3(t,y)
global mal msg Cpal Cpsg Cvwv Cpwa Cpair mair MWw R2 V Tev Tcd Troom
Taincool Tainhot dUadsorption dHevap UA UAlost
dy=zeros(5,1);
```

```
dy(1)=-
radsorption(y(1),y(2),y(3))*msg*MWw*R2*y(2)/V+y(1)/y(2)*(q(Tainhot,y(2))-
qlost(y(2),Troom)-
radsorption(y(1),y(2),y(3))*msg*dUadsorption)/(mal*Cpal+msg*Cpsg+y(1)*V/(MW
w*R2*y(2))*Cvwv+y(3)*msg*Cpwa);
dy(2)=(q(Tainhot,y(2))-qlost(y(2),Troom)-
radsorption(y(1),y(2),y(3))*msg*dUadsorption)/(mal*Cpal+msg*Cpsg+y(1)*V/(MW
w*R2*y(2))*Cvwv+y(3)*msg*Cpwa);
dy(3)=radsorption(y(1),y(2),y(3));
dy(4)=q(Tainhot,y(2));
dy(5)=qlost(y(2),Troom);
%Y=[P T L Qacc Qacclost]
```

Event Function to Terminate Step 3

```
function [value,isterminal,direction] = events3(t,y)

global Pcd

value = y(1)-Pcd ;     % Detect height = 0
isterminal = 1;   % Stop the integration
direction = 0;   % Both direction
```

ODE Function of Step 4, Continue Desorption

```
function dy=Step4(t,y)
global mal msg Cpal Cpsg Cvwv Cpwa Cpair mair MWw R2 V Tev Tcd Troom
Taincool Tainhot dUadsorption dHevap UA UAlost
dy=zeros(5,1);
dy(1)=0;
dy(2)=(q(Tainhot,y(2))-qlost(y(2),Troom)-
radsorption(y(1),y(2),y(3))*msg*dUadsorption)/(mal*Cpal+msg*Cpsg+y(1)*V/(MW
w*R2*y(2))*Cvwv+y(3)*msg*Cpwa);
dy(3)=radsorption(y(1),y(2),y(3));
dy(4)=q(Tainhot,y(2));
dy(5)=qlost(y(2),Troom);
%Y=[P T L Qacc Qacclost]
```

Function to Calculate Adsorption Rate

```
function Y=radsorption(XP,XT,XL)

global R1

%Define constant for adsorption reaction
%radsorption=k0*exp(-Ea/RT)*(L*-L)
k0=261145.0/60; %1/sec
Ea=34621.4; %J/mol


Y=k0*exp(-Ea/R1/XT)*(Leq(XP,XT)-XL);
```

Function to Calculate Equilibrium Water Uptake

```
function Y=Leq(XP,XT)

%Define constants for equilibrium uptake of silica gel
%Leq=A*(P/Psat)^B
%A=A0 + A1.T + A2.T^2 + A3.T^3
%B=B0 + B1.T + B2.T^2 + B3.T^3

A0=1.396E1;
A1=-8.876E-2;
A2=1.771E-4;
A3=-1.022E-7;
B0=1.010E3;
B1=-8.850;
B2=2.590E-2;
B3=-2.528E-5;

A=A0+A1*XT+A2*XT^2+A3*XT^3;
B=B0+B1*XT+B2*XT^2+B3*XT^3;
Y=A*(XP/Psat(XT))^B;
```

Function to Calculate Saturated Water Vapor Pressure

```
function Y=Psat(XT)

Y=760*10^(-7.90298*(373.16/XT-1)+5.02808*log10(373.16/XT)-1.3816e-
7*(10^(11.344*(1-XT/373.16))-1)+8.1328e-3*(10^(-3.49149*(373.16/XT-1))-1));
```

Function to Calculate Rate of Heat Transferred to the Device

```
function Y=q(XTi,XTw)

global UA mair Cpair

XTo=(XTi-XTw)/exp(UA/mair/Cpair)+XTw;
Y=UA*(XTi-XTo)/log((XTi-XTw)/(XTo-XTw));
```

Function to Calculate Rate of Heat Lost from the Device

```
function Y=qlost(XTw,XTr)

global UAlost

Y=UAlost*(XTw-XTr);
```